Textural analysis and emplacement conditions of well-preserved Orosirian felsic volcanic rocks of Northern Amazon Craton, Brazil

Carla Joana Santos Barreto[a*], Mauricio Barcelos Haag[b,c], Jean Michel Lafon[d], Carlos Augusto Sommer[b], Lúcia Travassos da Rosa-Costa[e]

[a] Departamento de Geologia, Universidade Federal de Pernambuco. Av. Arquitetura s/n, Recife-PE, Brazil.

[b] Instituto de Geociências, Universidade Federal do Rio Grande do Sul. Av. Bento Gonçalves 9500, Rio Grande do Sul-RS, Brazil.

[c] Department of Earth Sciences, University of Toronto. 22 Ursula Franklin Street, Toronto, ON, M5S 3B1, Canada.

[d] Instituto de Geociências, Universidade Federal do Pará. Rua Augusto Corrêa 1, Belém-PA, Brazil.

[e] Serviço Geológico do Brasil, Companhia de Pesquisa de Recursos Minerais, Av. Perimetral 3645, Belém-PA, Brazil.

* corresponding author: carla.barreto@ufpe.br

Graphical Abstract

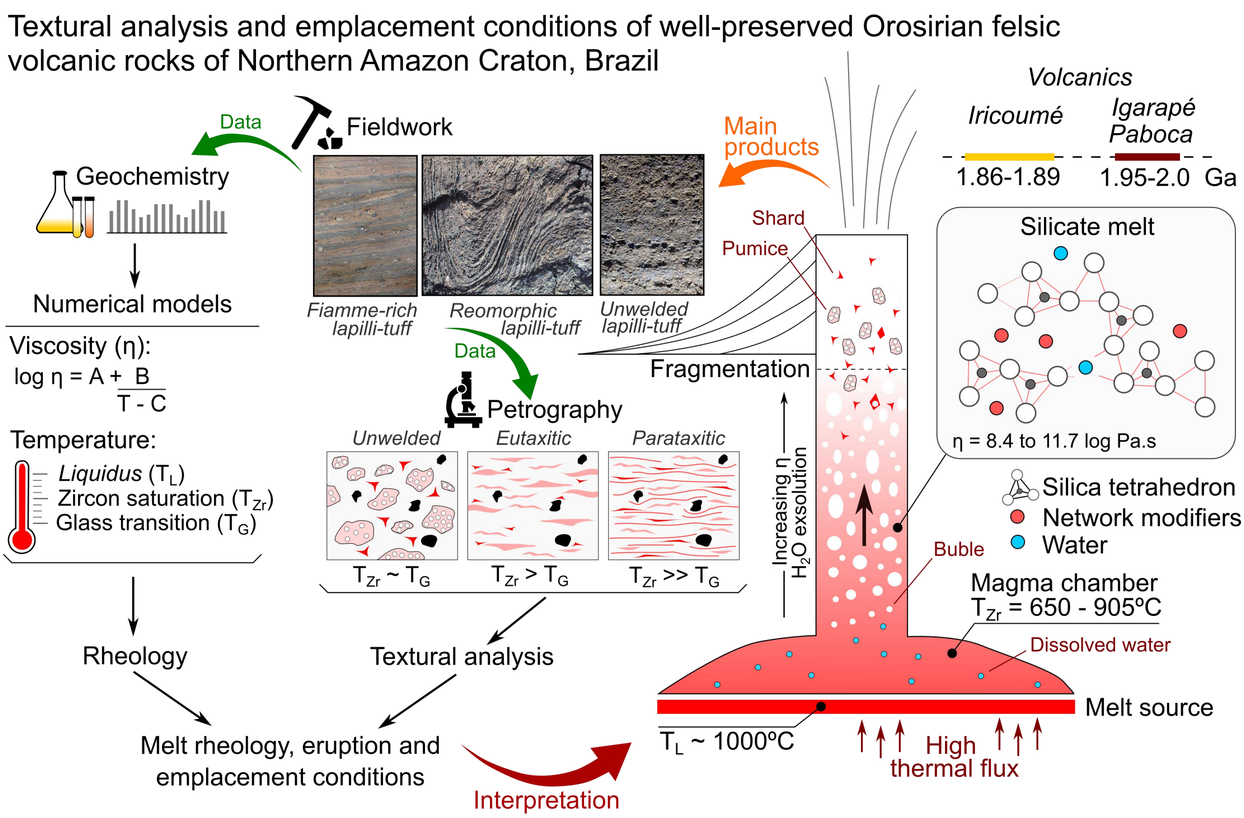

Abstract

Located in the Amazon Craton, the Uatumã magmatism (1.89-1.87 Ga) consists in one of the oldest Silicic Large Igneous Provinces (SLIPs) on Earth. For a long time, the access to these deposits in the northern Amazon Craton (Erepecuru–Trombetas Domain) has been set back for volcanological studies due to dense vegetation cover and the absence of roads. Recent studies identify two Orosirian volcanic units in the region: the Iricoumé Group (1.89-1.87 Ga) related to the Uatumã magmatism, and the Igarapé Paboca Formation (1.99-1.94 Ga), associated to an older magmatism. Both units are widespread in the Erepecuru–Trombetas Domain and include effusive and explosive deposits. In this paper, we apply textural analyses and rheological estimations to determine the eruption and emplacement conditions of these two volcanic sequences. Textural analyses were carried out through fieldwork and petrography, including a systematic classification of lavas and volcaniclastic rocks. Rheological parameters were determined using geochemistry data to obtain melt viscosity (η) and temperature, zircon saturation (T_{Zr}), liquidus (T_L), and glass transition temperatures (T_G), for anhydrous and hydrous compositions. Textural analyses indicate the predominance of volcaniclastic facies with abundant eutaxitic and parataxitic textures. Rheological estimations reveal T_L of 1020ºC, T_{Zr} 650-905ºC, and T_G 640-753ºC for anhydrous Iricoumé Group melts. Eruptive viscosity estimations range from 8.4 to 11.7 log η (Pa.s). Igarapé Paboca melts present higher temperatures, with T_L of 1050ºC, T_{Zr} 710-880ºC, and T_G 670-740 ºC. Modeling using hydrous compositions indicate that minute amounts of water can strongly affect the rheology of the studied melts, reducing η, T_L, T_{Zr}, and T_G. The petrographic features indicative of hydrous magma reinforces the role of H_2O as a controlling agent in the fragmentation of Iricoumé and Igarapé Paboca melts. The pyroclastic samples are marked by elevated ΔT_{Zr} - T_G relationships indicative of high emplacement temperatures above the T_G. Our results indicate that the high temperatures and the presence of network-modifier cations in the studied melts favored the development of extensive welded ignimbrites associated with low-eruption columns, likely developed in fissural and/or caldera systems.

Keywords: Orosirian volcanism; Felsic ignimbrite; Magma rheology; Amazon craton; Welding; Silicic Large Igneous Province.

1. Introduction

Located in the northeastern section of South America (Fig. 1A), the Amazonian Craton consists of the largest Precambrian domain in the South American Platform (Almeida et al., 1981). This terrane hosts some of the most important mineral deposits of the world (e.g., Juliani et al., 2005; Bettencourt et al., 2016; Motta et al., 2019), as well as a significant geological record of the Paleoproterozoic period. The widespread Uatumã volcano–plutonic event (1.89-1.87 Ga) covers 1.2 million km^2 of the Amazonian Craton (Fig. 1B, Guiana and Brazil Central shields) and is considered by several authors a Silicic Large Igneous Province (SLIP; Teixeira et al., 2019 and references therein). This Orosirian magmatic province is considered one of the most intriguing magmatic events of the world, with abundant explosive, effusive and intrusive rocks that are still poorly constrained due to dense vegetation cover (Schobbenhaus and Brito Neves, 2003; Brito Neves, 2011; Fernandes et al., 2011; Juliani et al., 2011; Klein et al., 2012; Barreto et al., 2013, 2014; Roverato et al., 2019; Teixeira et al., 2019).

The Guiana Shield represents the northern portion of the Amazonian Craton, to the north of the Amazon Basin (Fig. 1B). This area has been subdivided into several tectonic-geochronological provinces (Santos et al., 2000, 2006; Tassinari and Macambira, 2004) and tectonic–stratigraphic domains based on geological, geochronological, structural and geophysical data (Reis et al., 2003, 2006; Vasquez and Rosa-Costa, 2008). Located in the Brazilian part of the central-south Guiana Shield, the Erepecuru–Trombetas Domain (Fig. 1A) documents two Orosirian magmatic events separated by 100 Ma. These events include the Uatumã magmatism, which volcanic rocks have been grouped in the Iricoumé Group (1.89-1.87 Ga), and an older volcanism, related to Orocaima Event, grouped in the Igarapé Paboca Formation (1.99-1.94 Ga) (Castro et al., 2014; Silva et al., 2019). Both the Iricoumé Group and the Igarapé Paboca Formation consist of explosive and effusive volcanic rocks of felsic to intermediate compositions with well-preserved textures and structures that record the dynamics of this volcanism.

For a long time, access to these units and the Erepecuru–Trombetas Domain was hampered for systematic geological and geochronological studies due to the scarcity of roads. As a result, studies on the Uatumã magmatism have been concentrated in Tapajós and Iriri-Xingu domains, in the Brazil Central Shield (Fig. 1B - e.g. Lamarão et al., 2002; Fernandes et al., 2006; Juliani and Fernandes, 2010; Fernandes et al., 2011; Semblano et al., 2016; Lagler et al., 2019; Roverato et al., 2019) and in the Pitinga mining district of the Uatumã-Anauá Domain (Fig. 1B - e.g. Ferron et al., 2010; Pierosan et al., 2011a, 2011b; Simões et al., 2014a). Recent geological mapping performed by the Geological Survey of Brazil (Castro et al. 2014; Silva et al., 2019) in addition to petrographical, geochemical, and geochronological studies (Barreto et al., 2013, 2014; Leal et al., 2015, 2018; Silva et al. 2019) improved the geological knowledge of this domain. However, investigations of emplacement mechanisms and volcanic processes in the Erepecuru–Trombetas Domain are still scarce.

This study aims to improve the current knowledge about the volcanic rocks of the Iricoumé Group and the Igarapé Paboca Formation in the southern-central Guiana Shield. In order to achieve this purpose, we applied textural analysis to define coherent and volcaniclastic facies. For volcaniclastic samples, we also established a ranking of welding intensity. To explore the conditions of emplacement of the ancient Uatumã SLIP and older volcanics, we used geochemical data to obtain temperature and viscosity estimations using zircon saturation, liquidus, and glass transition temperatures. Based on textural features and the rheological parameters, we determine the eruption and emplacement mechanisms of the Iricoumé Group and Igarapé Paboca Formation to reconstruct part of the Orosirian volcanism.

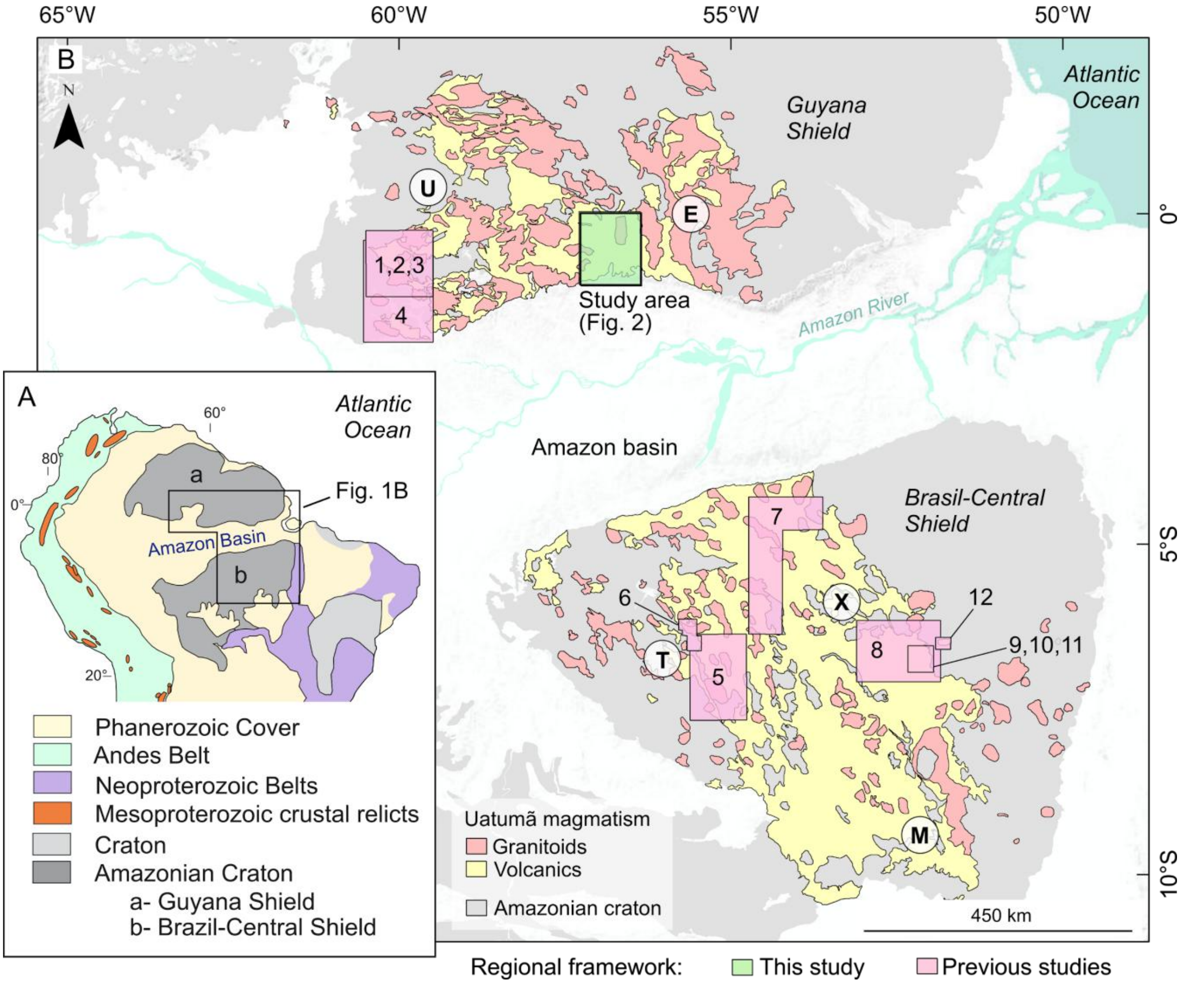

Fig. 1. A) Map of South America highlighting the Amazonian Craton and its subdivision into the a) Guiana Shield and the b) Brazil-Central Shield (modified from Fraga and Cordani, 2019); B) Occurrence of the Uatumã magmatism in the Amazonian craton, identified in the study area and previously studied regions: 1 - Ferron et al. (2010), 2 - Pierosan et al. (2011a), 3 - Pierosan et al. (2011b), 4 - Simões et al. (2014a), 5 - Roverato et al. (2019), 6 - Lamarão et al. (2002), 7 - Semblano et al. (2016), 8 - Roverato et al. (2019), 9 - Fernandes et al. (2006), 10 - Juliani and Fernandes (2010), 11 - Fernandes et al. (2011), 12 - Lagler et al. (2019). Tectonic Domains: U: Uatumã-Anauá; E: Erepecuru-Trombetas; T: Tapajós; X: Iriri-Xingu; M: North Mato Grosso. Based on Cordani et al. (2016).

2. Geological background

Located in the Amazon Craton, the Erepecuru–Trombetas Domain is constituted by Archean and/or Paleoproterozoic basement units (undifferentiated complex and volcano-sedimentary sequences), two Orosirian magmatic associations (ages ca. 2.0-1.95

Ga and 1.89-1.86 Ga), and Paleoproterozoic and Paleozoic sedimentary rocks. Undifferentiated mafic rocks, diabases, and nepheline syenites are also identified in the region (Vasquez and Rosa-Costa, 2008). The study area is located in the central-south segment of the Erepecuru–Trombetas Domain. In this area, two Orosirian magmatic associations are the dominant, whereas basement outcrops are absent. The available zircon U-Pb and Pb-Pb radiometric data on the Orosirian magmatic rocks of the Erepecuru-Trombetas domain are presented in Table 1.

Geological unit	Rock type	U-Pb zircon Age (Ma)	Pb-Pb zircon Age (Ma)	Ref.
	Old Orosirian magmatism			
Caxipacoré Suite	Syenogranite		1977 ± 4	1
	Monzogranite		1982 ± 9	1
	Quartz-monzonite	1986 ± 5		2
	Monzogranite	1986 ± 4		2
	Monzogranite	1991 ± 6		3
	Monzogranite	1989 ± 7		3
	Monzogranite	1995 ± 19		4
Igarapé Taboca Formation	Andesite		1992 ± 3	5
	Andesitic ignimbrite	1948 ± 6		2
	Uatumã magmatism			
Água Branca Suite	Monzonite	1887 ± 5		3
Mapuera Suite	Granite	1881 ± 8		3
	Granite		1889 ± 2	6
	Granite		1861± 20	6
Iricoumé Group	Andesite	1889 ± 9		2
	Trachydacitic Ignimbrite		1888 ± 3	5
	Trachydacitic Ignimbrite		1889 ± 2	5

Table 1. Zircon U-Pb and Pb-Pb radiometric data on the Orosirian magmatic rocks of the Erepecuru-Trombetas Domain. References: 1. Leal et al. (2015); 2. Silva et al. (2019); 3. Leal et al. (2018); 4. Vianna et al. (2017); 5. Barreto et al. (2013); 6. Castro et al. (2014).

The older magmatic association (2.0-1.95 Ga) is constituted by granites included in the Caxipacoré Suite and volcanic rocks (effusive and pyroclastic) of the Igarapé Paboca Formation. The Caxipacoré Suite consists of alkali feldspar granites, syenogranites, monzogranites, and granodiorites, whereas the Igarapé Paboca Formation comprises andesites, dacites, and subordinate trachyandesites, trachytes, ignimbrites, tuffs, and breccias.

Both volcanic and plutonic rocks present a high-K to shoshonitic, calc-alkaline signature related to arc-setting (Barreto et al., 2014; Leal et al., 2018; Silva et al., 2019). The Caxipacoré granitoids show U-Pb and Pb-Pb zircon ages around 1.96-1.99 Ga (; Leal et al., 2015, 2018; Silva et al., 2019; Vianna et al., 2017), whereas the Igarapé Paboca Formation displays U-Pb and Pb-Pb zircon ages between 1.99 and 1.95 Ga (Barreto et al., 2013; Castro et al., 2014; Silva et al., 2019).

The younger volcano-plutonic association (1.89-1.86 Ga), related to the Uatumã event, is constituted by granitic rocks of Água Branca and Mapuera suites and the volcanic rocks of the Iricoumé Group. Both granitoid suites and the Iricoumé volcanics are considered coeval (Table 1 and Fig. 2). However, the Iricoumé Group and Mapuera Suite, (which predominate in the study area) share similar geochemical characteristics that are distinct from the Água Branca granitoids (Barreto et al., 2014; Leal et al., 2018; Silva et al., 2019). The granitoids of the Mapuera Suite comprise alkali feldspar granites, syenogranites, and monzogranites with A-type affinity. Pb-Pb and U-Pb zircon ages range between 1889 ± 2 and 1861 ± 20Ma (Castro et al., 2014; Leal et al., 2018; Silva et al., 2019).

The Iricoumé Group is composed of undeformed and unmetamorphosed effusive, pyroclastic, and subvolcanic volcanic rocks of felsic to intermediate composition with K-high calc-alkaline to shoshonitic signatures and A-type magma affinity. The available geochronological Pb-Pb and U-Pb zircon data for these rocks suggest a narrow range of volcanism ages, from 1.89-1.88 Ga (Barreto et al., 2013; Silva et al., 2019).

The 1.89-1.88 Ga Uatumã volcanism has been studied in detail in several domains of the Amazon Craton (e.g., Costi et al., 2000; Klein and Vasquez, 2000; Reis et al., 2000, 2006; Lamarão et al., 2002, 2005; Almeida, 2006; Fernandes et al., 2006, 2011; Ferron et al., 2006, 2010; Valério et al., 2009; Pierosan et al., 2011a, 2011b; Klein et al., 2012; Barreto et al., 2013, 2014; Marques et al., 2014). The designation of Iricoumé Group is used for volcanic rocks outcropping in the Erepecuru-Trombetas and Uatumã-Anauá domains to the north of the Amazon Basin. To the south of this basin, correlated volcanic rocks occur in the Iriri-Xingu Domain under the designations of Sobreiro and Santa Rosa formations (Fernandes et al., 2006, 2011; Roverato, 2016; Roverato et al., 2017). In the Tapajós Domain, the correlated volcanic rocks are grouped in the Moraes Almeida Formation of the Iriri Group (Klein and Vasquez, 2000; Lamarão et al., 2002; Juliani et al., 2005).

Several undifferentiated small mafic rock bodies intrude rocks of the Iricoumé Group and Igarapé Paboca Formation. Geochronological data is still not available for these rocks, which has been interpreted by Vasquez and Costa (2008) as intra-plate mafic magmatism related to either Orosirian (≈1.88 Ga) or Statherian (≈1.78 Ga) crustal extension.

The Urupi Formation outcrops in the study area as an elongated ridge with NW–SE direction. This sedimentary formation includes sandstones, arkoses, and siltstones intercalated with volcaniclastic rocks (silicified tuffs and ignimbrites). The maximum age for this formation has been established at ca. 1.88-1.86 Ga based on the ages of the underlying Iricoumé volcanic rocks. Minimum age of 1.78 Ga was obtained with the U-Pb zircon dating of diabase sills, which are intrusive in the Urupi Formation (Santos et al., 2002). Recently, two groups of U-Pb LA-ICPMS ages of 2167-2050 Ma and 2761-2574 Ma were obtained for detrital zircons of the Urupi Formation, (Magalhães et al., 2017).

The Trombetas Group is composed of sandstones, shales, and siltstones that correspond to the early stages of Paleozoic deposition of the Amazon Basin with transgressive-regressive characteristics. As field data are lacking, the available information about this unit was obtained from remote-sensing interpretations (Silva et al., 2019). The rocks of this group occur in the southern limit of the studied region and show a pronounced relief with well-fitted drainage and V-shaped valleys, which contrasts with the low-relief of the Precambrian units of the Igarapé Paboca Formation and the Iricoumé Group.

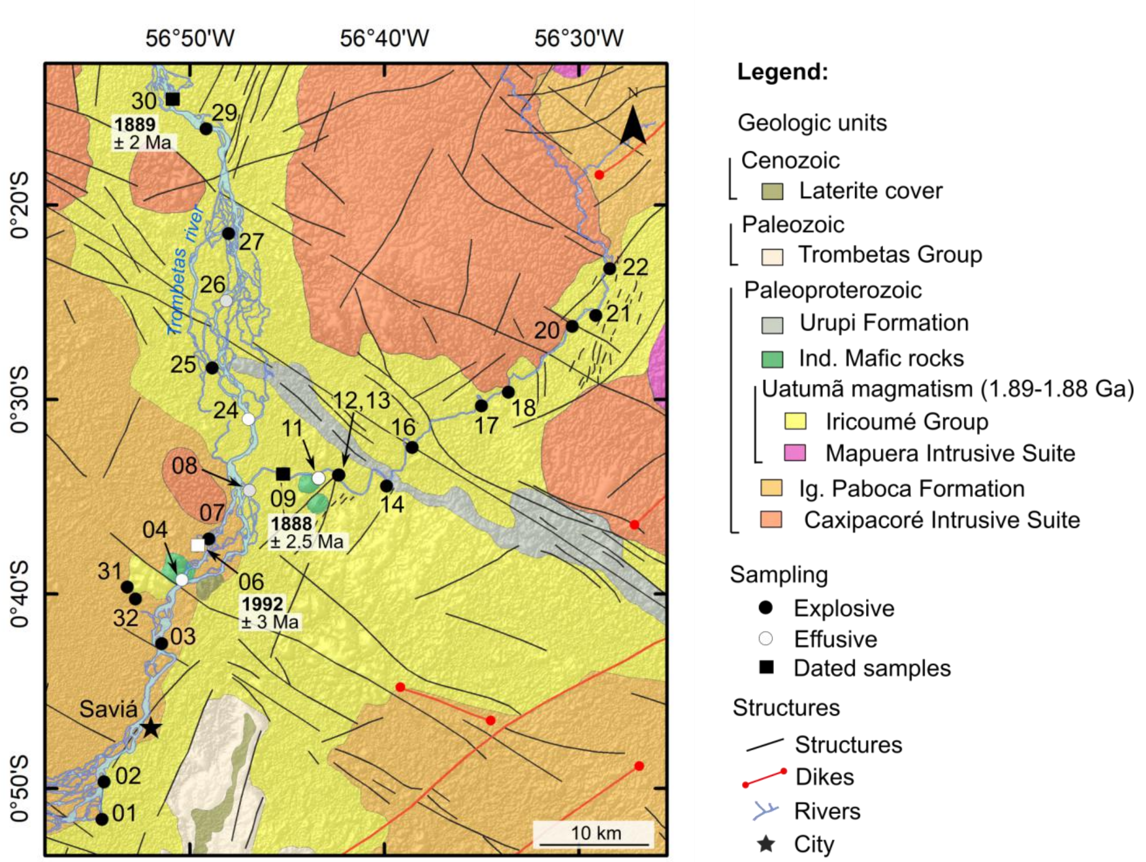

Fig. 2. Location map (see also Fig. 1B) with sampling sites and main geologic units. For a sample list of geological units, please check Table 2. Geochronological data from Barreto et al. (2013). Map modified from Silva et al. (2019), shaded relief derived from ALOS PALSAR digital elevation model (https://vertex.daac.asf.alaska.edu/).

3. Methods

3.1 Petrography

The fieldwork was performed by SBG-CPRM team during the project of mapping of the Pará state (Castro et al., 2014; Silva et al., 2019). For this study, the CPRM-Belém provided the outcrop photographs and samples. From the most representative samples, 18 thin sections were prepared and described using a Leica DM4500 digital microscope model with an attached camera (LEICA DFC495 model).

3.1.1 Ranking welding intensity

To compare our volcaniclastic samples, we present a scheme for ranking welding intensity in pyroclastic rocks, which comprises five ranks (I-IV) defined according to macroscopic and microscopic textural characteristics. Our classification is based on the Quane and Russel (2004) scheme to characterize welding intensity, with some modifications in order to highlight the differences observed in the studied samples. Our scheme includes incipiently welded (rank I), moderately welded with eutaxitic texture (rank II), and strongly welded with parataxitic texture (rank III). The petrographic descriptions used to define each rank as well as the equivalences with the scheme from Quane and Russel (2004) are listed in Table 2. Field and petrography data are depicted in Figures 3 to 7 to illustrate the textural categories and the main characteristics of each rank.

3.2 Whole-rock geochemistry

The studies of textural analysis and imaging were performed in 18 samples of the Erepecuru-Trombetas Domain, including 3 hypabyssal rocks, 2 lavas, and 13 ignimbrites rich in juvenile fragments. The whole-rock chemical analyses of these samples were performed at ACME Laboratories Ltd (Vancouver, Canada). Major oxides were obtained by inductively coupled plasma atomic emission spectrometry (ICP-AES), while the zr trace element was analyzed by inductively coupled plasma atomic mass spectrometry (ICP-MS). The analytical protocol at the ACME laboratory included the analysis of standard STD SO-18 and BLK and of three sample duplicates (LT-03, LT-13, and LT-32). The representative geochemical results are presented in Table 2 and plotted in the SiO_2 vs Zr/TiO_2 classification diagram (Fig. 8) using the GeoChemical Data toolkit v. 2.3 software (available at http://www.gcdkit.org/gcdkit-publications/).

3.3 Rheology

Based on geochemical data, we estimated rheological parameters for the ignimbrites and lavas of the Iricoumé Group and Igarapé Paboca Formation (Table 3) using the numerical models of Watson and Harrison (1983), Sisson and Groove (1993), and Giordano et al. (2008).

We applied the model of Watson (1979) and Watson and Harrison (1983) to estimate magma temperatures using the zircon saturation geothermometer (T_{Zr}). The Zircon saturation method has been successfully applied to igneous and volcanic rocks, allowing the determination of transport and emplacement mechanisms (e.g., Liu et al., 2013). We used the model of Sisson and Groove (1993) to determine the liquidus temperature (T_L), which represents the magma generation temperature and can give clues about the geotectonic and thermal regime of the region.

The model of Giordano et al. (2008) was applied to calculate the melt viscosity (η) and the glass transition temperature (T_G). While T_L indicates the maximum temperature, T_G reflects the boundary temperature between a ductile (above T_G, allowing viscous flow, pyroclastic sintering, and welding) and a fragile (below T_G, allowing only elastic deformation) behavior of a silicate melt (Webb, 1997; Giordano et al., 2005). A detailed description of rheological calculations is given in Supplementary material A, B, C, and D.

All mentioned parameters were estimated using both anhydrous and wet compositions with 0.25, 1.0, 2.0, and 4.0 wt% of H_2O, to evaluate the effect of dissolved magmatic water on the studied melts.

4. Results

4.1. Field and faciological aspects

Ignimbrites are the main volcanic deposits in the area and are characterized by eutaxitic and parataxitic textures (Fig. 3A-3C) with low to moderate inverse grading (Fig. 3D). These rocks are generally moderately to poorly sorted, with fragment sizes ranging up to lapilli (Fig. 3E) of plagioclase, sanidine, and quartz crystals, as well as sub-angular to sub-rounded lithic clasts and pumices (Fig. 3F). The groundmass of these deposits generally includes pumices and fiammes (Fig. 3A, 3B, 3C, 3F) and sometimes fiammes with spherulitic texture (Fig. 3G). Subordinately, some samples of crystal-rich ignimbrites also occur in the studied area and are characterized by crystal contents of up to 40% (vol.), mainly composed of quartz and feldspar (Fig. 3H).

The rheomorphic ignimbrites show subhorizontal bands (Fig. 4A), boudinage fiamme characterizing the parataxitic texture, and sometimes tight isoclinal folds at the outcrop scale (Fig. 4B-4C). These rheomorphic ignimbrites show angular-shaped broken crystal fragments of plagioclase and lithic clasts with sizes ranging from ash to lapilli (Fig. 4D). Often these ignimbrites show all fiamme collapsed and the parataxitic texture is faintly visible, which could led to a false interpretation of porphyritic texture (Fig. 4D).

Minor occurrences of effusive deposits, including lava and subvolcanic rocks, have been described in close association with the explosive deposits. The lavas are crystal-rich andesitic and show massive structure as well as porphyritic texture, characterized by high concentration (more than 35% vol.) of plagioclase and amphibole phenocrysts (Fig. 4E).

The subvolcanic rocks comprise two groups of rocks: lamprophyres and dacites. The lamprophyres are massive and porphyritic, characterized by amphibole phenocrysts set in an aphanitic matrix (Fig. 4F). Dacitic rocks exhibit flow-foliations at outcrop scale (Fig. 4G) and alkali feldspar and plagioclase porphyries set in an aphanitic groundmass at a macroscopic scale (Fig. 4H).

Fig. 3 (below). Field photographs of the ignimbrites of the Iricoumé Group and Igarapé Paboca Formation. A-C) Hand-samples showing pumices and fiammes characterizing the eutaxitic and parataxitic textures. The pumices and fiammes are marked with white arrow (samples LT-22, LT-25, LT-20); D) ignimbrite showing weak inverse grading (sample LT-22); E) Poorly sorted ignimbrite with ash and lapilli-sized fragments (sample LT-20); F) Detail of hand-sample showing the crystal fragments of plagioclase, sanidine, and quartz (yellow arrow), as well as pumices in the groundmass (red arrow) and lithic clasts (red dotted area) (sample LT-30); G) bands of fiamme devitrified to spherulitic texture. Some spherical spherulites are marked with red arrow (sample LT-02); H) crystal-rich ignimbrites characterized by high crystal contents of quartz and feldspar (yellow arrow) and pumices (white arrow) (sample LT-09).

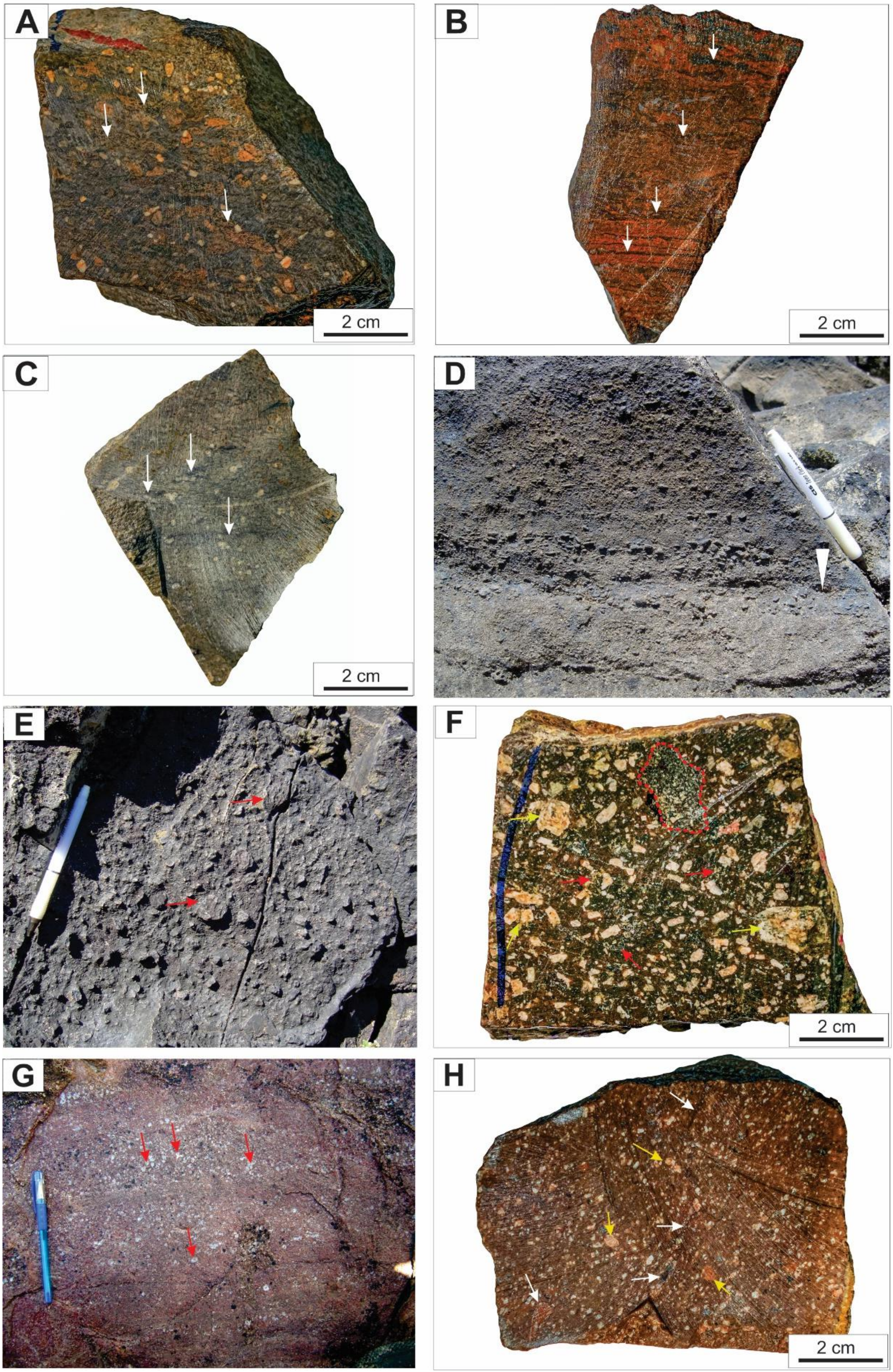

293

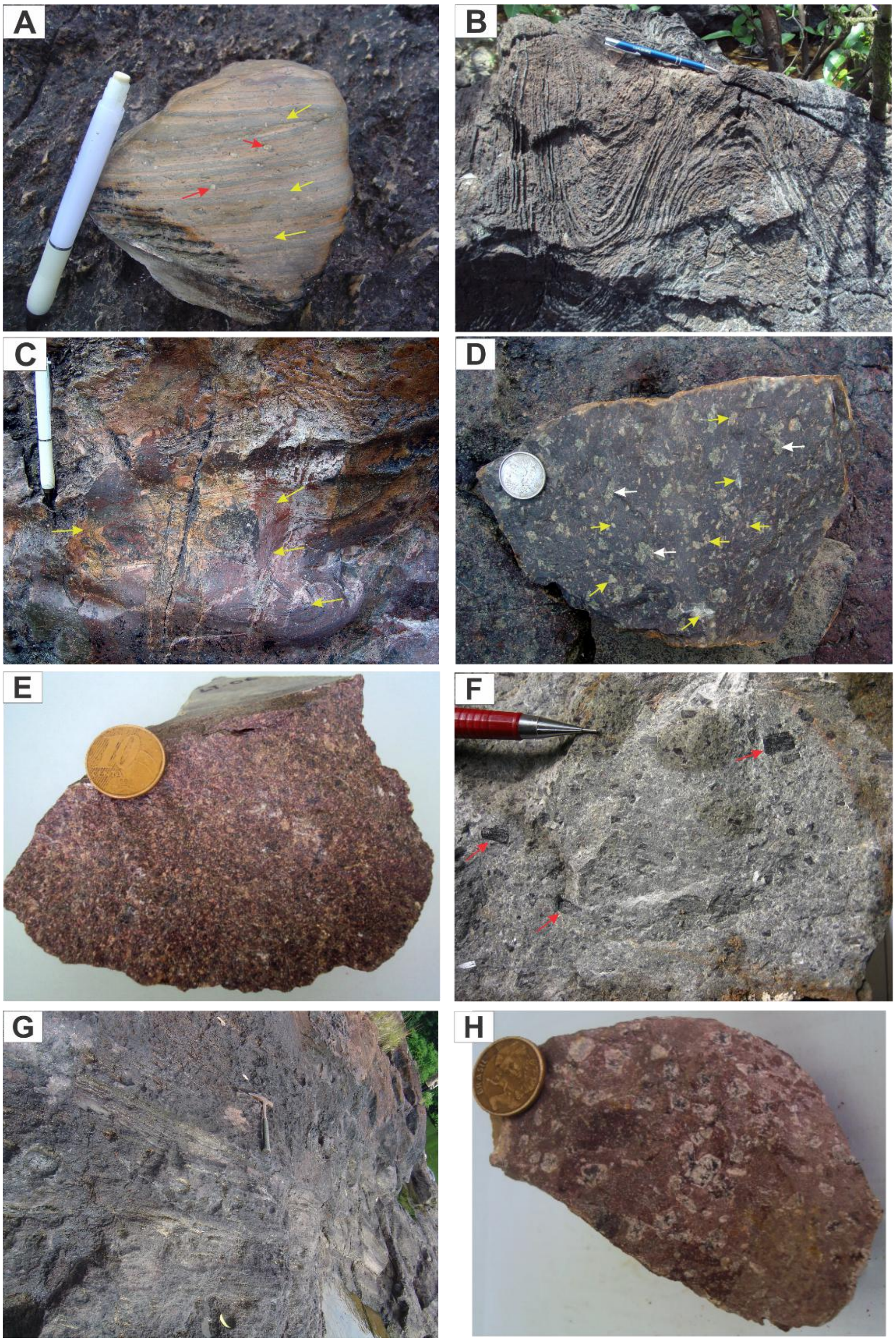

294

295 **Fig. 4**. Field photographs of the explosive and effusive volcanic rocks of the Iricoumé Group and Igarapé Paboca
296 Formation. A) Bands of rheomorphic ignimbrites characterized by angular-shaped crystal fragments of plagioclase and
297 fiammes (yellow arrow) characterizing the parataxitic texture (sample LT-25); B) Rheomorphic ignimbrite showing tight
298 isoclinal folds in field-scale (cf. Silva et al. 2019; sample LT-21); C) Detail of the fiammes and tight isoclinal folds in the
299 field-scale (yellow arrow) (sample LT-21); D) Rheomorphic ignimbrite showing all fiamme collapsed where the

parataxitic texture is faintly visible, which could led a false interpretation of apparent porphyritic. The crystal fragments of plagioclase and lithic clasts are highlighted by yellow and white arrows, respectively (sample LT-31); E) Crystal-rich lava with porphyritic texture, characterized by plagioclase and amphibole phenocrysts set in an aphanitic groundmass (sample LT-06); F) lamprophyre massive and porphyritic, characterized by amphibole phenocrysts (red arrow) set in an aphanitic matrix (sample LT-11); G) Flow-foliations in hypabyssal dacite (sample LT-08); H) Dacitic rock in hand-sample exhibiting alkali feldspar and plagioclase porphyries set in an aphanitic groundmass (sample LT-08).

4.2. Textural analysis

Volcanic rocks were divided into lavas and volcaniclastic facies and accordingly subdivided into five textural groups with different welding intensities for the pyroclastic deposits as shown in Table 2 and described below.

4.2.1. Volcaniclastic facies

Apparent porphyritic texture with granophyric groundmass (Incipient degree of welding - rank I)

The ignimbrites of this category show fragmental texture with low to voluminous (5 to 35 vol.%) poorly sorted angular to sub-rounded fragments of sanidine, plagioclase, and quartz characterizing an apparent porphyritic texture set in a granophyric groundmass made up of mosaic of quartz and feldspar (Fig. 5A, 5B). Some quartz fragments in the ignimbrites exhibit corrosion embayments, which indicate magmatic resorption (Fig. 5C). Subordinately, there are some samples of ignimbrites with high concentration of crystal fragments and lithic clasts (Fig. 5A, 5D, 5E).

The crystal fragments are set in this groundmass rich in slightly deformed pumice and devitrified glass shards (Fig. 5A-5E). The pumice fragments have ragged margins, with lenticular and blocky shapes and are completely altered to phyllosilicate minerals, ensuring preservation of their outlines (Fig. 5A-5G). Pumices are deformed with flame-like ends, especially around accidental lithic clasts and crystal fragments, such as quartz, plagioclase, and biotite (Fig. 5D-5F). Sometimes, the pumices encompass lithic clasts and crystal fragments (Fig. 5E), including biotite crystals completely pseudomorphosed by iron oxides (Fig. 5D-5E).

The glass shards observed in the groundmass are more easily recognized in plane polarized light and show incipient welding compaction and their shapes range from cuspate, Y-shaped, platy, curviplanar, blade-like, to pumice (Fig. 5C, 5F, 5G). Taking into account the vitroclastic texture produced by pyroclastic eruptions is no longer preserved in the matrix of these Precambrian ignimbrites, all the shapes of the shards were well preserved due to devitrification to fine-grained quartz-feldspar aggregates (Fig. 5G).

The granophyric texture was also described in the groundmass and is characterized by fine-grained amorphous quartz (cristobalite) and feldspar aggregates (Fig. 5B, 5H). This granophyric texture commonly overprints any pre-existing vitroclastic texture in the matrix and is the result of high-temperature devitrification processes as well as the spherulitic texture that is also present (Fig. 5G).

According to the incipiently welded texture of the pumices, these rocks belong to rank I in the welding intensity, which is equivalent to grades II and III of classification of Quane and Russel (2004).

FACIES	SAMPLE	TEXTURAL CATEGORY	RANK		WELDING INTENSITY	INTERPRETATION OF PROCESS	FIGURES
			Literature[1]	This study			
VOLCANICLASTIC			I				
	LT-09, LT-12, LT-29	Apparent porphyritic with cryptocrystalline groundmass	II	I	The glass shards are only slightly deformed. The pumices are incipiently flattened and welded and no eutaxitic texture is observed. The glassy material (shards and pumices) are completely devitrified	The weak deformation of pyroclasts suggests the beginning of the welding in the ash matrix and pumice lapilli and a pyroclastic origin for these deposits [2]	3F,3H, 5A-5H
	LT-03*, LT-20		III				
	LT-30, LT-21, LT-22, LT-18	Eutaxitic	IV	II	The glass shards are moderately adhered to one another and individual shards are moderatly deformed. Rocks moderately to strongly welded with a clear eutaxitic texture showing moderately deformed pumices as well as fully collapsed fiamme	The eutaxitic texture record hot deformation of pyroclasts and is generated by increasing welding process involving syn or post-emplacement degassing, compaction, annealing and flow of glassy material in pyroclastic deposits[2]	Fig. 3A, 3D, 3G, 6A-6F
	LT-01, LT-16	Parataxitic	V	III	densely welded with all fiamme collapsed. The strong eutaxitic texture change for parataxitic texture with features of folds, elongation lineations and boudins. Sometimes the obsidian-like fiamme are faintly visible or difficult to identify that resembles to texture of a lava	The parataxitic texture is formed when all the fiammes of a pyroclastic deposit suffer coalescence and are welded to obsidian-like vitrophyre, which remove the pore spaces. Development of pronounced elongation lineations, folds, kinematic indicators, and boudins indicate syn- and/or postwelding hot-state ductile shear deformation (process of reomorphism)[2]	Fig. 3B, 3C, 4A-4D, 7A-7F
	LT-25, LT-31*		VI				
COHERENT	LT-06*, LT-04*, LT-24, LT-11	Porphyritic and glomeroporphyritic with microcrystalline to pilotassitic groundmass				The porphyritic and glomeroporphyritic textures suggest emplacement of lava flows with crystallization in two stages and heterogeneous crystallization, respectively. The microcrystalline to pilotassitic textures of the groundmass indicate lack to intermediate movement of flow of the lava flows [3]	Fig. 4E, 4F, 8A, 8B, 8C, 8D
	LT-08, LT-26	Porphyritic and glomeroporphyritic with spherulitic groundmass				The porphyritic and glomeroporphyritic textures suggest emplacement of lava flows with crystallization in two stages and heterogeneous crystallization, respectively. The spherulitic texture of the groundmass indicate high-temperature devitrification [3]	Fig. 4G, 4H, 8E, 8F

Table 2. Summary of textural categories and rank of welding intensities of the volcanic rocks of the Iricoumé Group and Igarapé Paboca Formation. 1= Quane and Russel (2004); *= samples from the Igarapé Paboca Formation; 2= Branney and Kokelaar (2002); 3= Vernon (2004).

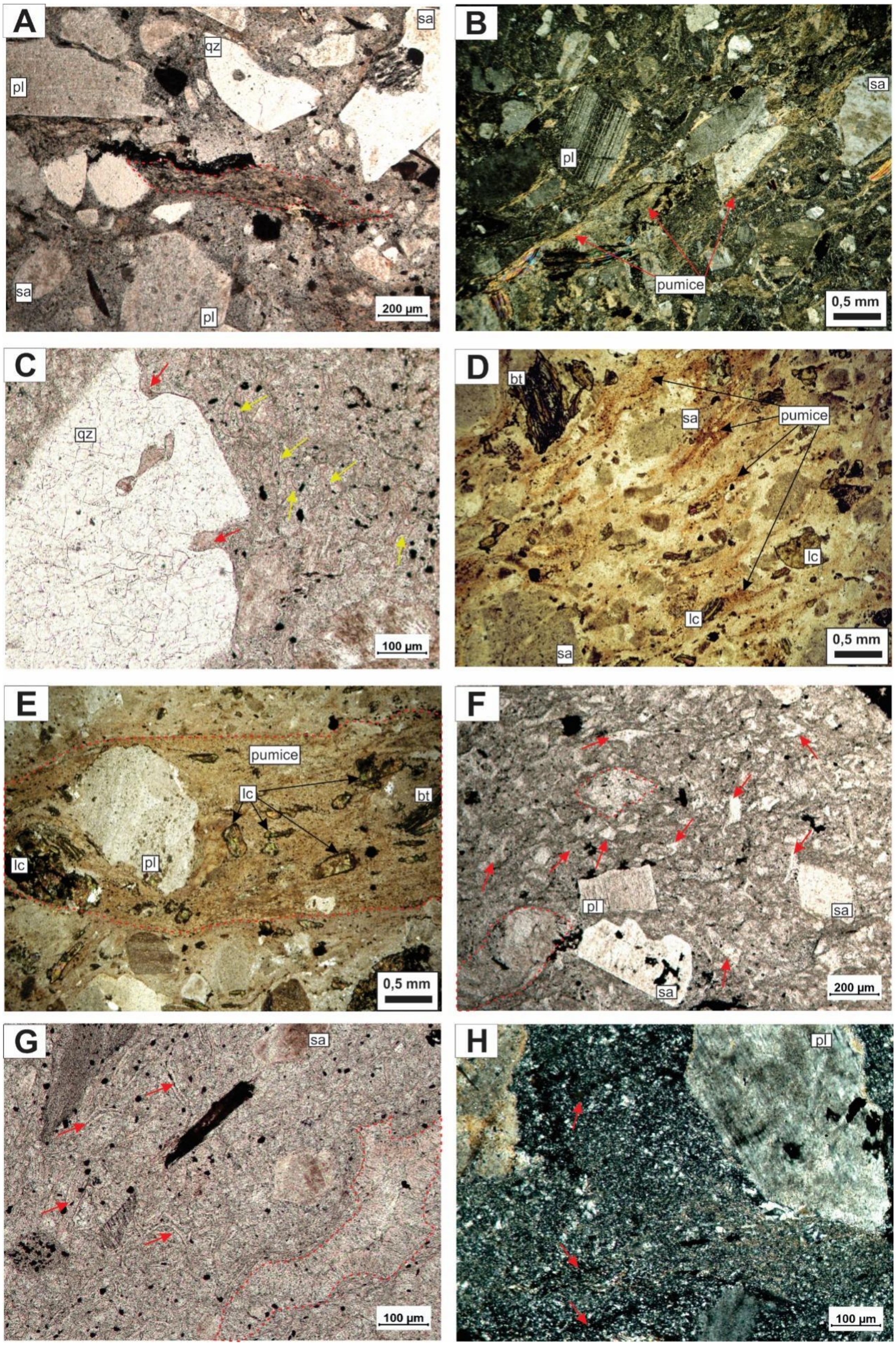

Fig. 5. Photomicrographs of the incipiently welded apparent porphyritic texture, which represents the rank I of the welding intensity. A) Crystal-rich ignimbrite characterized by angular fragments of plagioclase (pl), sanidine (sa) and quartz (qz) set in a groundmass with pumices (red dotted area) incipiently welded

(sample LT-09) - Parallel polarized light; B) Crystal-rich ignimbrite with fragmental texture and poorly sorted angular fragments of sanidine (sa) and plagioclase (pl) set in granophyric groundmass with slightly deformed pumice and altered to phyllosilicates (sample LT-12) – Crossed polarized light; C) Ignimbrite showing quartz fragment with corrosion embayment (red arrow) set in a groundmass with glass shards (yellow arrows) (sample LT-03) – Parallel polarized light; D) Pumice fragments show lenticular shapes and ragged margins deformed around sanidine crystals (sa) and lithic clasts (lc) and are completely altered to phyllosilicate minerals, ensuring preservation of their outlines. Biotite crystals are completely pseudomorphosed by iron oxides (sample LT-29) – Parallel polarized light; E) Pumices with blocky shape that encompass accidental lithic clasts (lc), plagioclase (pl) and biotite (bt) fragments (sample LT-29) – Parallel polarized light; F) Ignimbrite with poorly sorted fragmental texture defined by angular to sub-rounded fragments of sanidine (sa) and plagioclase (pl) in a groundmass rich in shards with shapes ranging from cuspate, Y-shaped, platy, curviplanar (red arrow), to pumice (red dotted area) (sample LT-20) – Parallel polarized light; G) Detail of the well preserved outlines of the glass shards (red arrow) and spherulitic texture (red dotted area) in the matrix (sample LT-03) – Parallel polarized light; H) Pumice fragments (red arrow) and granophyric texture in the groundmass, characterized by fine-grained quartz-feldspar aggregates (sample LT-20) – Crossed polarized light.

Eutaxitic texture (moderate degree of welding - rank II)

Ignimbrites exhibit discontinuous foliation that alternates from light to dark colors, which reflects welding on different materials (Fig. 6A-6B). The ignimbrites are composed mainly of crystal fragments of sanidine, plagioclase, quartz, biotite, and strongly flattened fiamme fragments characterizing an eutaxitic texture (Fig. 6A-6E). Lenticular to disc-shaped fiamme have wispy, flame-like ends and are deformed, especially around rigid components (crystal fragments) (Fig. 6C-6F), in which some crystal fragments are rotated (Fig 6F). Lithic clasts are scarce in these ignimbrites.

The processes that obliterate the vitroclastic texture include high welding degree and alteration of fiamme to phyllosilicate minerals and quartz-feldspar aggregates (Fig. 6C).

Features of high-temperature devitrification are also observed generating the granophyric texture that comprises a fine-grained quartz-feldspar mosaic (Fig. 6D-6F).

Based on the eutaxitic texture of these ignimbrites that characterizes a moderate degree of welding of the pumices towards fiammes, these rocks are classified in the rank II of the welding intensity, which is equivalent to grade IV of classification of Quane and Russel (2004).

Fig. 6 (below). Photomicrographs of ignimbrites with eutaxitic texture, which represent the rank II of welding intensity. A) Ignimbrite with discontinuous foliation characterized by lenticular to disc-shaped fiammes (dark colors highlighted by red dotted line) (sample LT-21) – Parallel polarized light; B) Fiammes (red arrow) with lenticular shapes and sometimes deformed around sanidine (sa) fragment (sample LT-21) – Parallel polarized light; C) Fiammes altered to phyllosilicate minerals (red arrow) and quartz-feldspar aggregates (yellow arrow) (sample LT-21) – Parallel polarized light; D) Ignimbrite with crystal fragments of sanidine (sa), plagioclase (pl), quartz (qz), and strongly flattened fiammes characterizing the eutaxitic texture. Fiammes (yellow arrow) altered to phyllosilicates have flame-like ends and are deformed around crystal fragments (sample LT-18) – Crossed polarized light; E) Detail of the angular plagioclase (pl) and sanidine (sa) fragments rounded by fiammes deformed. Groundmass completely devitrified to fine-grained quartz-feldspar mosaic characterizing the granophyric texture is also present (sample LT-18) – Crossed polarized light; F) Detail of the rotated plagioclase fragment (red arrow) wrapped by fiammes altered to phyllosilicate (yellow arrow) (sample LT-18) – Crossed polarized light.

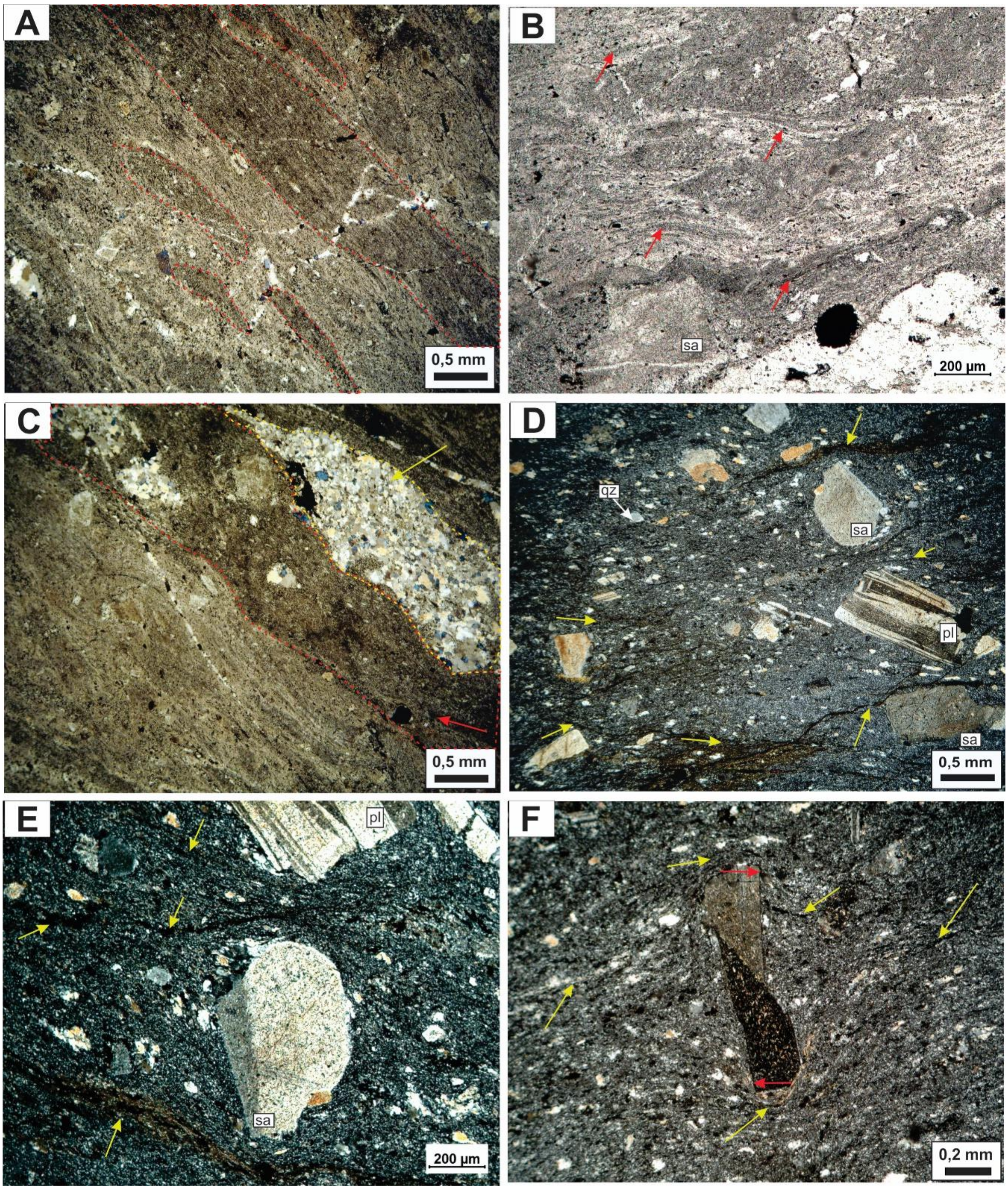

404

405 ***Parataxitic texture (high welding degree - rank III)***

406 The rheomorphic ignimbrites are characterized by broken crystal fragments of sanidine,
407 plagioclase, quartz, and amphibole within groundmass with densely welded fiammes that
408 are difficult to distinguish (Fig. 7A-7F). These ignimbrites commonly display high-

temperature devitrification of the formerly glassy components generating granophyric textures (Fig. 7C, 7D, 7F).

The amphibole crystals are partially to completely replaced by opaque minerals (Fig. 7A). The fiamme fragments show a reddish color due to oxidation (Fig. 7A, 7B, 7E) and are deformed and flattened around crystal fragments and cognate and accidental lithic clasts (Fig. 7A-7E).

The foliations developed in the rheomorphic ignimbrites define the parataxitic texture, characterized by strong welding and compaction of fiamme, which generate intrafolial folds in micro-scale and boudinage features (Fig. 7E), suggesting that the rheomorphic processes occurred during and/or after flow emplacement (Branney and Kokelaar, 2002). In most cases, this strong welding and compaction approaching homogenization generates a pattern of structures similar to magmatic foliations, typical of lavas (Fig. 7F).

Based on the parataxitic texture described in the rheomorphic ignimbrites, these rocks are classified in the rank III of the welding intensity, which is equivalent to grade V and VI of the classification of Quane and Russel (2004).

Fig. 7 (below). Photomicrographs of rheomorphic ignimbrite with parataxitic texture, which represent the rank III of welding intensity. A-B) Broken crystal fragments of sanidine (sa), plagioclase (pl), and opaque-altered amphibole (amp) within groundmass with densely welded fiammes that are difficult to distinguish. The fiamme fragments show a reddish tint in plane-polarized light due to oxidation and are deformed and flattened around lithic clasts and crystal fragments (samples LT-01 and LT-16) – Parallel polarized light; C-D) Strongly welded fiammes around crystal fragments of plagioclase (pl), sanidine (sa) and quartz (qz), and lithic clasts (lc). Note the granophyric texture in the devitrified groundmass (samples LT-01 and LT-16) – Crossed polarized light; E) The strong welding and compaction of fiammes (dark due to limited transparency under a petrological microscope) generate intrafolial folds in micro-scale (blue arrow) and boudinage features (red arrow) (sample LT-25) - Parallel polarized light; F) The strong welding and compaction of the rheomorphic ignimbrites led to the approaching homogenization generating a pattern of textures similar to magmatic foliations, typical of lavas. Note the granophyric texture in the devitrified groundmass (sample LT-31) – Crossed polarized light.

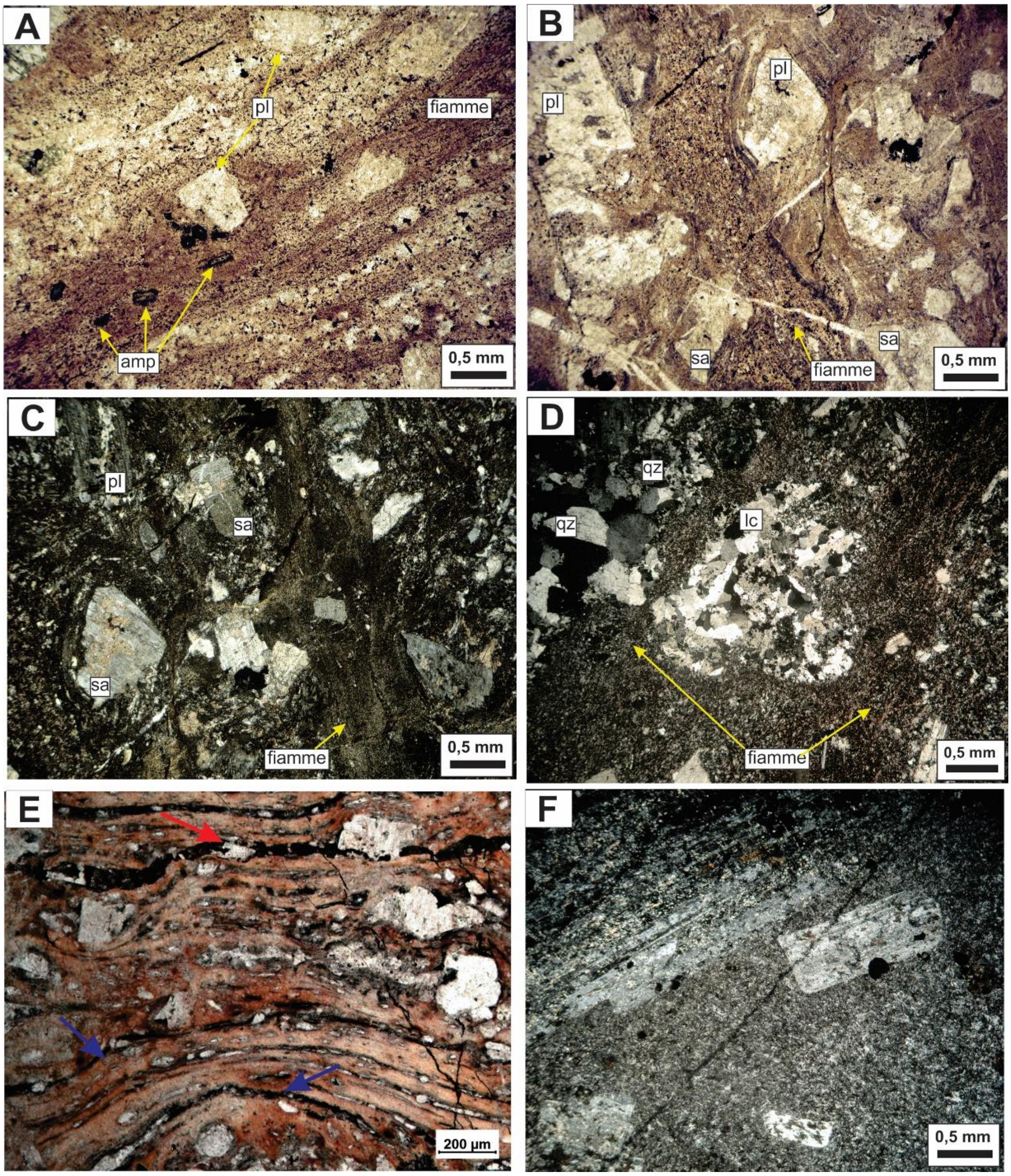

4.2.2. Lavas

Porphyritic and glomeroporphyritic texture with microcrystalline to pilotaxitic groundmass

The andesitic lavas and hypabyssal lamprophyres of andesitic composition show porphyritic and glomeroporphyritic textures characterized by 30-50% (vol.) of phenocrysts set in a groundmass of high crystallinity (Fig. 8A-8D).

The lavas show voluminous (35-50% vol.) phenocrysts of plagioclase and hornblende immersed in a microcrystalline groundmass, where predominate plagioclase microlites and small crystals of hornblende (Fig. 8A). All plagioclase crystals exhibit subhedral shapes and are moderately to strongly replaced by clay minerals, carbonate, and epidote. Hornblende phenocrysts show subhedral to sub-rounded shapes and are partially to completely replaced by opaque minerals (Fig. 8B).

The lamprophyres exhibit hornblende phenocrysts that reach up to 30% (vol.) set in a pilotaxitic groundmass, characterized by plagioclase microlites aligned in sub parallel mode along with hornblende microphenocrysts (Fig. 8C). Hornblende phenocrysts show subhedral to sub-rounded shapes, sometimes as aggregates in addition to zoning, simple twinning, and opacitic rims (Fig. 8C). Some crystals are partially to completely replaced by chlorite and opaque minerals, while others are partially corroded (Fig. 8D). All plagioclase crystals show subhedral shapes and are slightly replaced by clay minerals and epidote. The fact that these lamprophyres exhibit hornblende as the only mafic mineral and plagioclase > alkali feldspar (Le Maitre, 2002) allows classify them as spessartite.

Porphyritic and glomeroporphyritic texture with spherulitic groundmass

The dacitic subvolcanic rocks show porphyritic and glomeroporphyritic textures, characterized by plagioclase, quartz, and sanidine phenocrysts immersed in a glassy matrix (Fig. 8E-8F).

The plagioclase phenocrysts show shapes ranging from subhedral to euhedral and are partially altered to sericite, carbonate, and clay minerals. The sub-rounded sanidine porphyry exhibit carlsbad twinning, microperthites and are slightly- to moderately altered to sericite (Fig. 8E). Features of corrosion embayment are observed in the quartz and sanidine phenocrysts as a result of partial reabsorption processes (Fig. 8E). The matrix has undergone high-temperature devitrification processes generating spherulitic texture with axiolite, spherical, and fan-type spherulites (Fig. 8F).

Fig. 8 (below). Textural groups of the effusive deposits. A) Lava showing porphyritic texture characterized by plagioclase and hornblende phenocrysts immersed in a microcrystalline groundmass composed by plagioclase microlites and small crystals of hornblende (sample LT-24) – Crossed polarized light; B) Hornblende phenocrysts of the lavas show subhedral to sub-rounded shapes and are partial to completely altered for opaque minerals (sample LT-06) – Parallel polarized light; C) Lamprophyre exhibit porphyritic texture defined by hornblende phenocrysts set in a pilotassitic groundmass, characterized by plagioclase microlites aligned in sub parallel mode. Hornblende phenocrysts with subhedral to sub-rounded shapes show zoning (yellow arrow), simple twinning (red arrow), and opacitic rims (sample LT-04) – Crossed polarized light; D) Most of the hornblende phenocrysts range from partially to completely replaced by opaque minerals (yellow arrow), while some are partially corroded (green arrow) (sample LT-11) – Crossed polarized light; E) Hypabyssal dacite with glomeroporphyritic texture composed by plagioclase (pl) and microperthitic sanidine (sa) porphyries with sub-rounded shapes and corrosion embayment (red arrow) set in a spherulitic groundmass (sample LT-08) – Crossed polarized light; F) Detail of the fan (yellow arrow) and spherical-type (red arrow) spherulites scattered in the spherulitic groundmass (sample LT-26) – Crossed polarized light.

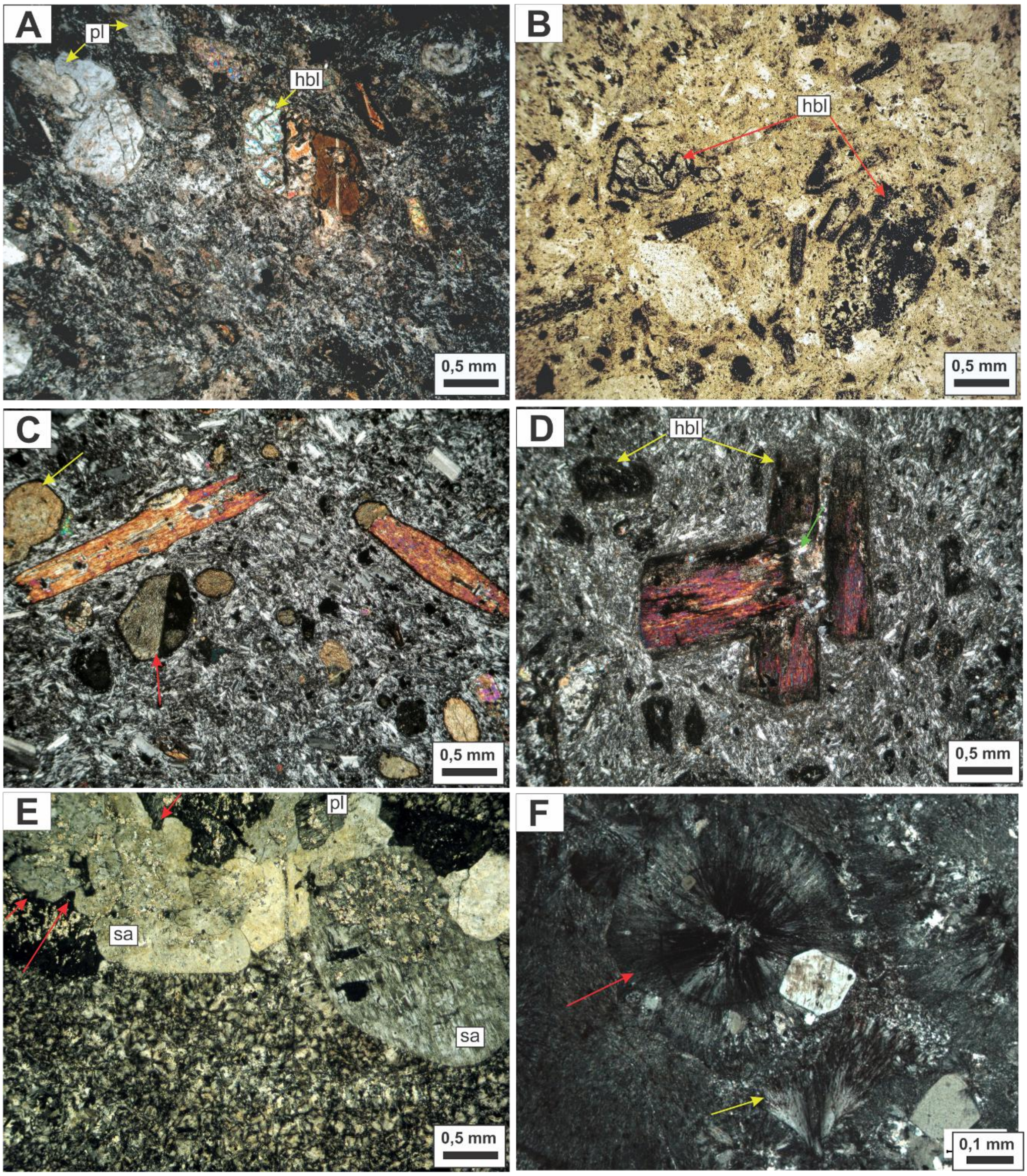

4.3. Geochemistry

Eighteen volcanic rocks representative of the Iricoumé Group and Igarapé Paboca Formation were analyzed for whole-rock geochemistry, including 13 ignimbrites, two lavas, and three hypabyssal rocks (Table 3). From this set, most of the samples are related to the Iricoumé Group, except by two pyroclastic rocks (samples LT-03 and LT-31) and one lava (sample LT-06) that belong to Igarapé Paboca Formation and are marked with an asterisk in table 2.

Barreto et al. (2014) described in detail the geochemical characteristics of major and trace elements of the volcanic rocks of this sector of the Erepecuru-Trombetas Domain. The high values of Loss on Ignition (LOI) obtained in some studied rocks (c.f. Table 2 of Barreto et al., 2014) due to weathering did not allow their classification in the Total-Alkali ($Na_2O + K_2O$) versus silica (TAS) diagram, as recommended by the International Union of Geological Sciences (IUGS). As a better alternative for the classification of altered volcanic rocks, we used the Zr/TiO_2 versus SiO_2 diagram (Winchester and Floyd, 1977) that establishes a relationship between major and trace elements with low degree of mobility (Fig. 9). In this diagram, the pyroclastic rocks occupy the dacite and rhyolite fields, while the lava domes show andesitic composition and the hypabyssal rocks range from andesitic to dacitic compositions.

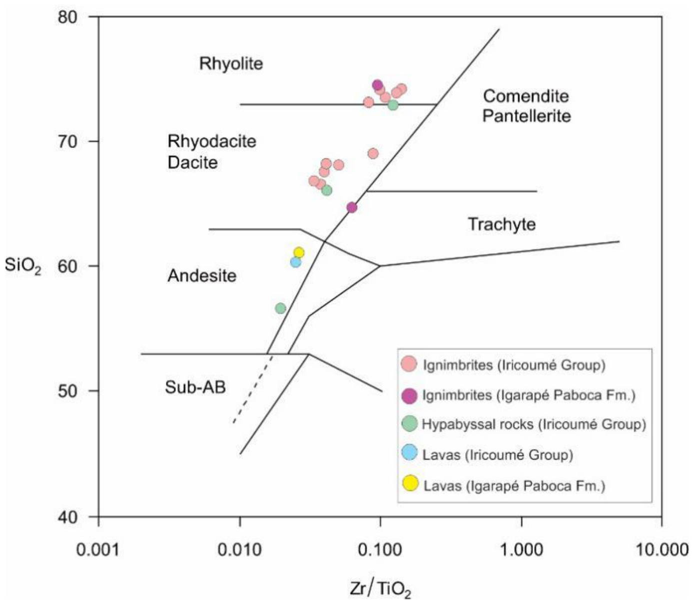

Fig. 9. SiO_2 versus Zr/TiO_2 classification diagram (Winchester and Floyd, 1977). Fm.= Formation. The pyroclastic rocks of the Igarapá Paboca Formation are the purple circles, while the lava of this unit is represented by yellow circle.

4.4. Temperature and viscosity of magmas

The main rheological parameters calculated on basis in the geochemical data are shown in the Table 3. Our results indicate that, for anhydrous compositions, Iricoumé Group melts present uniform T_L ranging from 920 to 1110 ºC (average of 1020 ºC), without significant T_L differences among explosive and effusive samples (Fig. 10A). Overall, samples of the Igarapé Paboca Formation display higher temperatures, with an average T_L of 1050 ºC (Fig. 10A). Zircon saturation temperatures (T_{Zr}) of Iricoumé Group display large variations from 707 to 905 ºC (average of 810 ºC, Fig. 10A).

The calculated viscosities at T_{Zr} span from 8.4 to 11.7 log η (Pa.s) (Fig. 10B), indicative of the *non-Arrhenius* behavior of these melts (Giordano et al., 2006). Comparing samples with similar silica content (SiO_2 % wt), several explosive samples tend to show significantly higher viscosities at T_{Zr} when compared to effusive samples (Fig. 10B). This difference can reach two orders of magnitude (i.e., 100 more viscous) in some cases.

When considering only pyroclastic samples of the Iricoumé Group, it is possible to observe high, virtually uniform T_L, and variable T_{Zr}, ranging from 729 to 871 ºC, while T_G ranges from 690 to 753 ºC (Fig. 10C). In the pyroclastic samples of Iricoumé Group, the ΔT_{Zr} - T_G ranges from 14 to 165 ºC (Fig. 10D), with several samples (> 70%) presenting high ΔT_{Zr} - T_G values (> 80 ºC), indicative of a high welding potential for the pyroclastic deposits of the Iricoumé Group. Explosive samples from the Igarapé Paboca Formation also display high ΔT_{Zr} - T_G values, which is attested by moderate to intense welding observed in these samples (Fig. 10D). This proxy also indicates that some samples were emplaced only a few degrees above the glass transition temperature, generating unwelded deposits. When compared to petrographic data and the ranking welding intensity based on the modified scale from Quane and Russell (2004), pyroclastic samples show a systematic increase in welding intensity as a function of $\Delta T_{Zr} - T_G$ (Fig. 10D), suggesting the ability of the $\Delta T_{Zr} - T_G$ proxy in predicting welding degree in the pyroclastic samples.

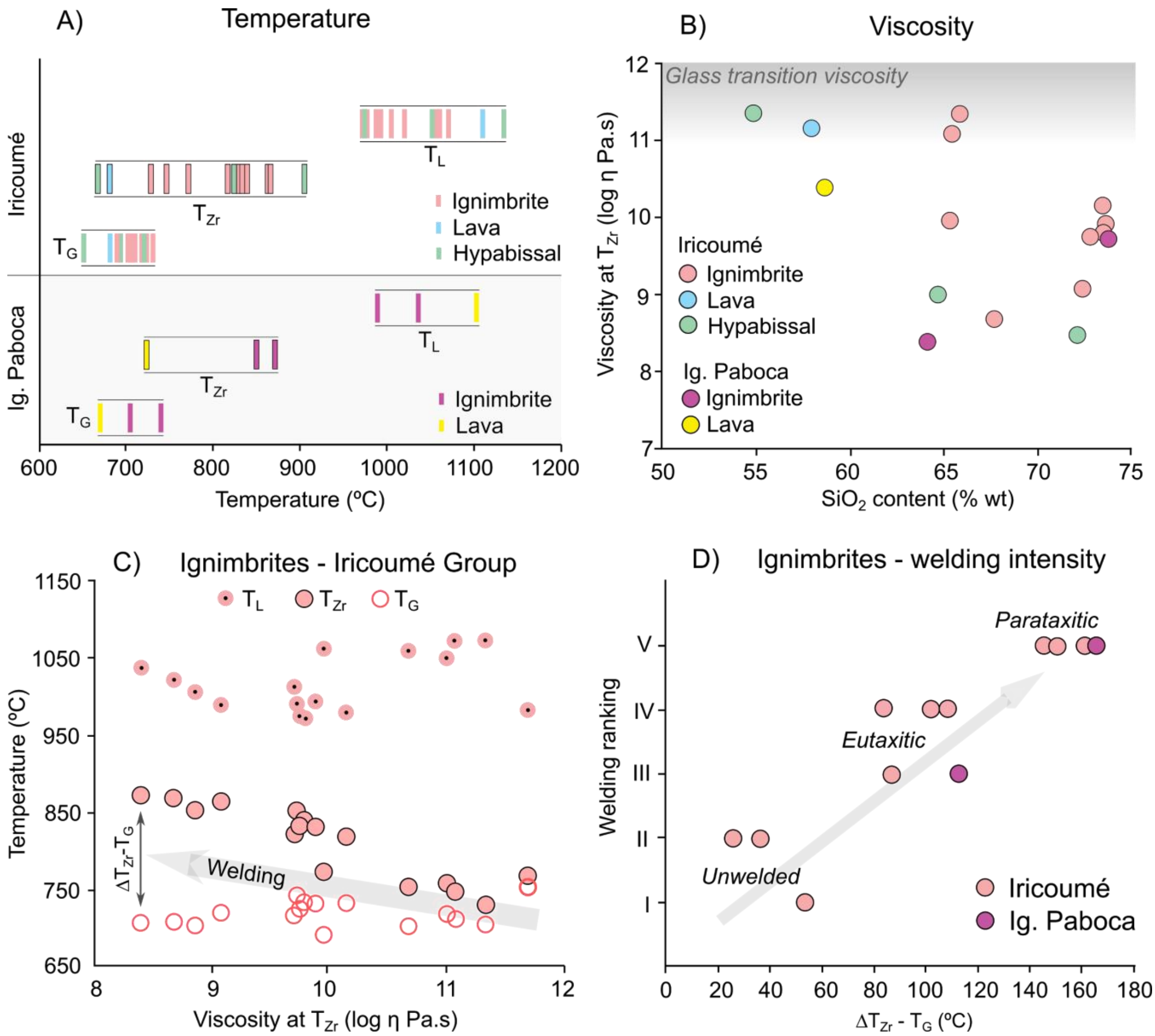

Fig. 10. Rheological results for Iricoumé and Igarapé Paboca melts: A) temperature results for the studied units, T_L , T_{Zr} and T_G; B) melt viscosity at T_{Zr} versus silica content; C) T_{Zr} and T_G versus melt viscosity of explosive samples from Iricoumé Group; D) petrographic welding ranking versus welding potential for ignimbrites of the Iricoumé Group and the Igarapé Paboca Formation. Geochemical data from Barreto et al. (2014) and partly displayed in the table 3.

Identification		Main network forming		Main network modifiers				Anydrous (0% H_2O)					0.25% H_2O			0.50% H_2O			1.00% H_2O			2.00% H_2O			4.00% H_2O		
Type	Sample	SiO_2	Al_2O_3	Na_2O	K_2O	P_2O_5	Zr (ppm)	TL (°C)	log η at TL (Pa.s)	T Zr (°C)	log η at T Zr (Pa.s)	TG (°C)	TL (°C)	log η (Pa.s)	TG (°C)	TL (°C)	log η (Pa.s)	TG (°C)	TL (°C)	log η (Pa.s)	TG (°C)	TL (°C)	log η (Pa.s)	TG (°C)	TL (°C)	log η (Pa.s)	TG (°C)
Explosive (Pyroclastic)	LT-01 (D)	67.48	15.96	4.47	6.17	0.19	288	1005	6.67	852	8.85	702	996	6.00	636	988	5.63	594	971	5.19	537	938	4.68	462	872	4.14	363
	LT-09 (D)	66.25	15.24	5.00	3.54	0.18	149	1058	5.81	753	10.67	701	1050	5.24	638	1041	4.91	596	1025	4.52	542	991	4.09	471	925	3.64	380
	LT-12 (D)	65.45	15.59	4.43	3.61	0.18	141	1071	5.76	747	11.08	711	1063	5.18	648	1055	4.87	608	1038	4.48	553	1005	4.04	482	939	3.60	391
	LT-16 (D)	67.69	15.27	4.56	5.48	0.11	451	1020	6.54	867	8.68	707	1011	5.89	641	1003	5.54	600	987	5.10	543	953	4.60	468	887	4.08	371
	LT-29 (D)	65.84	15.73	4.72	3.72	0.20	127	1071	5.62	729	11.33	704	1063	5.05	640	1055	4.74	601	1038	4.36	546	1005	3.94	476	939	3.51	388
	LT-30 (D)	65.31	15.35	4.65	4.39	0.21	157	1061	5.55	772	9.96	690	1053	5.00	627	1045	4.69	586	1028	4.32	533	995	3.91	464	929	3.49	375
	LT-31 (T)*	64.11	16.13	3.78	5.96	0.29	507	1036	6.07	871	8.40	706	1027	5.44	641	1019	5.11	601	1003	4.70	546	970	4.25	475	903	3.79	384
	LT-03 (R)	73.78	13.72	3.35	5.42	0.04	279	989	7.63	851	9.71	740	980	6.91	674	972	6.50	631	956	6.01	572	922	5.44	494	856	4.83	390
	LT-18 (R)	73.64	13.88	4.38	4.26	0.05	237	992	7.41	830	9.88	730	983	6.71	663	975	6.31	621	959	5.83	563	925	5.28	485	859	4.69	382
	LT-20 (R)	73.48	14.60	4.51	3.95	0.03	184	978	7.58	817	10.14	731	970	6.86	665	962	6.45	623	945	5.96	564	912	5.39	486	846	4.79	383
	LT-21 (R)	73.51	13.58	3.50	5.54	0.02	248	972	7.71	838	9.78	732	963	6.98	665	955	6.57	623	939	6.07	564	906	5.50	486	839	4.90	383
	LT-22 (R)	72.82	13.71	4.40	4.47	0.04	240	974	7.54	831	9.75	724	966	6.82	657	958	6.43	616	941	5.93	558	908	5.37	479	842	4.78	377
	LT-25 (R)	72.43	14.30	4.74	4.81	0.05	330	988	7.27	863	9.07	718	980	6.57	651	971	6.18	609	955	5.71	551	922	5.16	473	855	4.57	370
Effusive (Hypabyssal)	LT-11 (A)	54.86	14.57	4.50	2.03	0.45	155	1134	3.08	668	11.37	652	1125	2.71	595	1117	2.53	561	1101	2.32	518	1068	2.15	468	1001	2.10	411
	LT-08 (D)	72.09	14.74	4.16	5.72	0.04	434	974	7.51	905	8.47	721	966	6.79	654	958	6.38	612	941	5.89	553	908	5.33	475	842	4.72	371
	LT-26 (D)	64.67	16.23	4.96	4.38	0.23	270	1052	5.72	825	8.99	694	1044	5.15	631	1035	4.82	590	1018	4.43	535	986	4.00	465	919	3.56	375
Effusive (Lava)	LT-06 (A)	58.66	15.31	4.97	3.41	0.37	183	1104	4.33	724	10.41	671	1096	3.86	610	1087	3.61	572	1071	3.31	523	1038	3.01	462	972	2.74	387
	LT-24 (A)	57.90	15.45	3.83	3.71	0.36	176	1110	4.24	707	11.19	682	1101	3.78	621	1093	3.53	585	1077	3.24	536	1043	2.96	477	977	2.73	406

Table 3. Table of some major elements and zr trace element already published by Barreto et al. (2014) and the summary of the main rheological parameters of the Iricoumé Group and Igarapé Paboca Formation rocks (present study). Composition: Andesite (A), Dacyte (D), Rhyolite (R), Trachyte (T).

5. Discussion

5.1. Eruptive dynamics

The methodology applied in this study allowed us to establish a set of diagnostic features that can be used to distinguish between volcaniclastic and coherent textural samples generated by explosive and effusive eruptive styles. The explosive deposits are largely dominant in the studied region and include slightly welded to rheomorphic ignimbrites.

The pyroclastic deposits present massive and stratified aspect and are composed of devitrified juvenile components (pumice, fiamme, and glass shards), and lithic clasts, and crystal fragments transported predominantly by pyroclastic density currents (PDCs) during explosive events (Manville et al., 2009) (Figs. 5-7). PDCs consist of gravity-driven mixtures of hot gas and volcanic particles (Branney and Kokelaar, 2002), and the alternation of massive and stratified deposits is a common characteristic in PDC deposits (Sulpizio et al., 2014). This arrangement reflects primary events of deposition of concentrated PDCs, dominated by granular flow regimes (Sulpizio et al., 2014). The presence of devitrified juvenile components represent an important textural feature to distinguish silicic lavas from ignimbrites in the ancient volcanic environment of the Amazonian Craton (Figs. 5F, 5G, 6C-6E).

In contrast, the effusive eruptive style responsible for the coherent textures is represented by lavas and hypabyssal rocks, which show distinctive characteristics when compared to the pyroclastic rocks. These characteristics include porphyritic texture with a relative abundance of phenocrysts in a microcrystalline and pilotaxitic groundmass, as well as the absence of broken crystals, juvenile pyroclasts (pumice, fiamme, glass shards), and welding foliations.

In both effusive and explosive deposits, textural variations of the crystal populations (phenocryst, microphenocryst, and microlite) suggest changes in the composition, temperature, viscosity, and H_2O content before and during the eruption. These magmatic changes produced textures such as resorption embayments, reaction rims, and devitrification features that can help us understanding the thermal evolution of the studied melts.

The presence of embayed and round outlines in quartz and sanidine phenocrysts in rhyolitic ignimbrites and hypabyssal dacites can be generated due to either semi-adiabatic magma ascent or magma mixing and mingling (Müller et al., 2003, 2005). In the adiabatic decompression, SiO_2 solubility of the phenocryst-rich magmas increases as the pressure decreases, and, as result, phenocrysts that were initially in equilibrium with the melt are partially resorbed in pre-eruptive conditions (McPhie et al., 1993). The hypothesis of magma mixing and mingling for the development of resorption embayments seems unlikely in the studied rocks, since the typical characteristics of this process, such as plagioclase-mantled K-feldspar, sieve textured plagioclase and mafic micro enclaves (Muller et al., 2005) are absent in the studied samples.

For the Iricoumé Group samples, the calculated T_L ranging from 920 to 1110 ºC provides an estimation of the magma generation temperature under anhydrous conditions. Additionally, T_{Zr} values indicate the upper temperature limits in the magma chamber before the eruption. Viscosity calculations at T_L range from 5.5 to 8.0 log Pa.s, considerably lower values when compared to the estimated viscosities at T_{Zr}, owing to the temperature contrast between T_L and T_{Zr} (Table 3).

In contrast, Igarapé Paboca Formation melts present even higher T_L and lower viscosities, which can be linked to the compositional differences between these two units (Table 3). Despite the strong effect of temperature on melt viscosity, the models used in this study account for the non-arrhenian behavior of silicate melts, allowing a more comprehensive evaluation of the compositional effect of the studied melts on magma rheology (Giordano et al., 2006, 2008).

Barreto et al. (2014) based on Nd isotopic data, showed that parental magmas of the Iricoumé Group may have originated from the melting of crustal sources, likely Rhyacian. This is in agreement with Bryan et al. (2002), who suggest that the occurrence of SLIPs requires partial melting of the crust, which is favored by the presence of hydrated, high-K calc-alkaline andesites and amphibolites. As a consequence, Iricoumé samples are predominantly composed of more evolved terms, such as rhyolites and dacites, which show considerable contents of network-forming elements such as Si, O_2, Ti, Al, and Fe (Barreto et al., 2014; Silva et al., 2019), in concordance with the observed high-viscosity values in this study (Fig. 10B).

5.1.1. Water effect on eruption dynamics

The high viscosities under anhydrous conditions (Fig. 11B) may suggest the presence of some viscosity-reducing agent to allow magma ascent and eruption of the studied melts. The presence of water in the studied magmas could be responsible for exponentially reducing the melt viscosity, accelerating the ascent process that leads to fragmentation by decompression.

Textural evidence for the presence of water in the magma consists of rimmed amphibole phenocrysts, sometimes completely replaced by oxides observed in the andesitic lavas, lamprophyres, and ignimbrites (Figs. 7A, 8A-8D). This reaction texture suggests dehydration processes during magma ascent, comprising release of vapor phase from the magma chamber and onset of explosive processes (Buckley et al., 2006; Roverato et al., 2017). The partial replacement of amphibole phenocrysts by magnetite-rich opacitic texture reinforces the role of dehydration reactions during fast magma ascent (Buckley et al. 2006, Cruz et al. 2014; Lagler 2019).

Other studies developed in the northern Amazonian Craton, in both Trombetas and Pitinga regions also identified the occurrence of amphiboles in the Iricoumé Group samples (Pierosan et al., 2011a; Silva et al., 2019). These findings seem to support a hydrous scenario for the volcanism of the Iricoumé Group, which could explain the explosive nature of this volcanism. Recent experiments by Forte and Castro (2019) have shown that H_2O may dictate the eruption dynamics, inducing overpressure and fragmentation in natural samples with H_2O contents as low as 1.4 wt.%, when heated above the T_G.

In rhyolite melts, the amount of dissolved water can reach values up to 6 wt.%, that strongly affect melt viscosity and eruption dynamics (Kohn, 2000; Gonnermann and Manga, 2012; Forte and Castro, 2019). Simulations of progressive hydrous compositions (0.25, 1.0, 2.0, and 4.0 wt% H_2O) of the studied samples show that even small additions of H_2O (< 1 wt.%) can lead to a considerable decrease of both melt viscosity (up to 2 order of magnitude, according to the model of Giordano et al., (2008)) and temperature (T_L and T_G) (Table 3 and Fig. 11A). The H_2O effect also seems to be stronger in more evolved magmas, where larger contrasts of viscosity and temperature among hydrous and anhydrous compositions of the same melt can be observed (Fig. 11A).

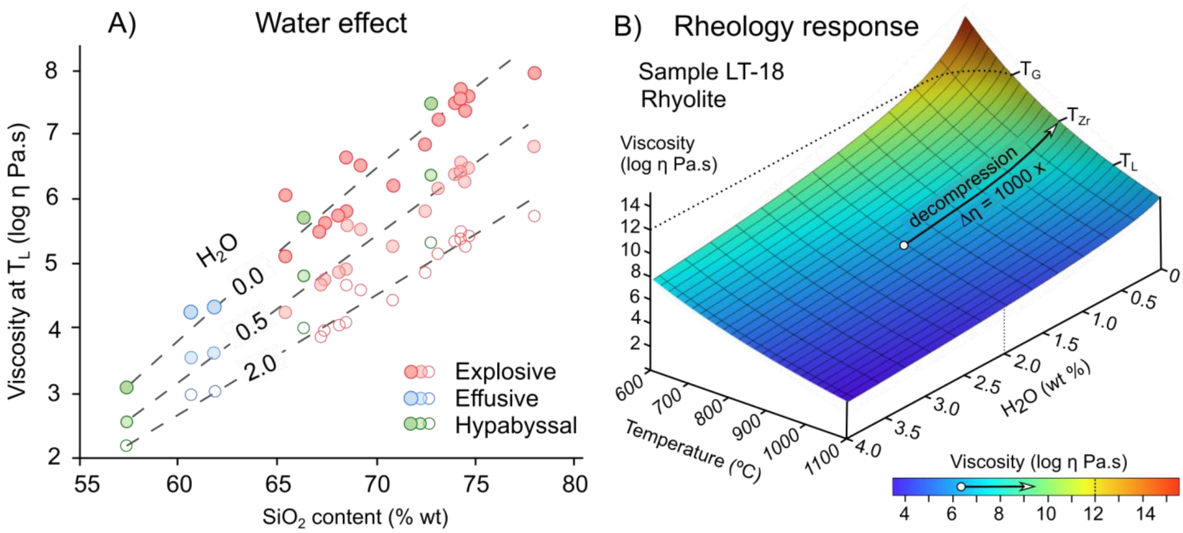

Fig. 10. Water effect on the studied melts: a) plot of H_2O effect on melt viscosity; b) rheological model showing the interplay among H_2O content, temperature, and viscosity. Δη = viscosity contrast during decompression.

To better understand the interplay of water content and temperature over magma rheology, we build a rheological model using a sample with an average composition of the Iricoumé Group (sample LT-18: rhyolitic ignimbrite). This model demonstrates the addition of 0.5 wt. % H_2O causes a change of viscosity equivalent to a temperature increase of 100 ºC (Fig. 10B; Grunder and Russell, 2005). This model also shows that, although the H_2O reduces the viscosity, the loss of this dissolved hypothetical H_2O due to sudden decompression may also lead to an increase up to a thousand times in melt viscosity (Δη in Fig. 11B), ultimately resulting in an explosive event.

The rheology calculations demonstrated that a considerable amount of magmatic water may be lost due to decompression and phase separation (Forte and Castro, 2019). Still, the remaining water can strongly affect the emplacement dynamics, reducing viscosity and T_G (Giordano et al., 2005) resulting in porosity loss and welding (Friedman et al., 1963; Grunder and Russell, 2005).

5.2. Emplacement conditions

5.2.1. Explosive products

The studied ignimbrites correspond to dense pyroclastic flow regime and show typical characteristics of mass flow-dominated deposits, such as massive aspect and poor sorting, characterized by angular fragments of juvenile components, crystals and lithic clasts. Crystal fragments record the fragmentation caused by the expansion of bubbles in the magma during the eruptive decompression (Best and Christiansen, 1997).

Rheological data suggest a predominance of high temperatures for the samples of the Iricoumé Group (T_{Zr} ranging from 729 to 867 ºC) and Igarapé Paboca Formation (T_{Zr} ranging from 851 to 871 ºC). These data are supported by field data with the predominance of welded, high-grade ignimbrites in the study area, which is in agreement with the other studies developed in rocks of the Iricoumé Group (Ferron et al., 2010; Pierosan et al., 2011a, 2011b; Barreto et al., 2013; Silva et al., 2019). This implies that several ignimbrites were deposited under high temperature conditions, above the calculated T_G, which allowed ductile deformation of juvenile pyroclasts (Branney and Kokelaar, 2002).

Additional evidence of high-temperature emplacement of the Iricoumé ignimbrites includes thermally oxidized pyroclasts, flow-foliations, and the widespread presence of eutaxitic (rank II) and parataxitic (rank III) textures. All these characteristics imply a hot, gas-supported flow emplacement in which turbulent shear-induced tractional segregation is suppressed (Branney and Kokelaar, 2002). Rapid chilling of silicate melt produces silicic glass, which may be replaced by spherulites and granophyric textures due to high-temperature devitrification and/or hydration (Logfren, 1970, 1971a, 1971b; Friedman and Long, 1984; Breitkreuz, 2013). Both effusive and pyroclastic rocks of the studied area display spherulitic textures including spherical, axiolite, fan-type spherulites, as well as granophyric. The types of devitrification textures can provide a clue to the history of the sub-solidus cooling under high-temperature conditions that occurred in the studied rocks (e.g., Logfren, 1971a, 1971b).

The first stage of devitrification consists of the development of abundant microlites and spherical spherulites (Logfren, 1971b). Swanson et al. (1989) defined that abundant small microlites represent metastable crystallization in response to a relatively high degree of undercooling. Lofgren (1971a) demonstrated that spherical spherulites form at low temperatures (< 400ºC), and their small diameters reflect a quick drop in temperature below the T_G, consistent with the rapid cooling rate. In contrast, spherulites of axiolite and fan types form at high temperatures (700ºC) and then are followed by a second devitrification stage, which is responsible for the development of granophyric texture (Lofgren, 1971a). As a result of these high-temperature processes, the ancient silicic volcanic rocks of the studied region are dominated by spherulitic or granophyric textural facies, which indicates that their groundmasses were formerly glassy, but now the glass is overprinted by devitrification and recrystallization to a quartz-feldspar mosaic due to later alteration (McPhie et al., 1993).

The incipiently welded ignimbrites with high crystals contents (apparent porphyritic texture with granophyric groundmass - rank I) occur in minor volume and display weak flow-foliations generated by welding. This high concentration of crystal fragments and lithic clasts (Fig. 5A, 5B, 5D, 5E) suggests the existence of elutriation processes of the glassy material of ash size in portions highly fluidized in the pyroclastic flow or even in the eruption column. This would lead to an accumulation of crystals and lithic clasts and the extraction of fine-down into secondary plumes during pyroclastic flow eruption and transport (Cas and Wright, 1987). The temperatures (T_{Zr}) in these ignimbrites are generally just a few degrees above the minimum welding temperature, i.e., the glass transition temperature (T_G), as observed in Fig. 10C. The large difference observed between T_L and T_G suggests that welding is possible in these cases, however, the high content of crystals in these ignimbrites inhibits more pronounced welding.

5.2.1.1. Welding

Historically, welding has been associated with processes of load-induced compaction and the rheological properties of the involved particles (Freundt, 1998; Branney and Kokelaar, 2002). More recently, this view has been challenged by the observation of deposits with complex welding patterns, including upward increasing in the welding degree (Soriano et al., 2002). In high-grade ignimbrites, the rheological parameters of the pyroclasts seem to play a major role, since low-viscosity particles can weld under minimal loading (Sumner and Branney, 2002).

The difference between emplacement and glass transition temperatures (ΔT_{Zr} - T_G) can be used as a proxy for welding potential, considering that the higher emplacement temperatures may result in more welded, high-grade ignimbrites. According to our rheological calculations, the studied ignimbrites show a progressive increase in welding intensity as a function of ΔT_{Zr}-T_G (Fig. 10D). This relationship implies a direct association between eruption temperatures and welding, suggesting either a proximal source for the ignimbrite deposits and/or an eruption column able to maintain high temperatures.

Using field and experimental data, Roche et al. (2016) showed that welding results from the deposition of sustained, dense PDCs. More recently, Pacheco-Hoyos et al. (2017) demonstrated that welding is mainly associated with little to no mixing with ambient air during flow, allowing high deposition temperatures and favoring viscous deformation of the pyroclasts.

The cooling rate of the pyroclasts also affects welding, since low cooling rates result in lower T_G, granting a wider welding window (Webb, 1997; Giordano et al., 2005). Low cooling rates can be achieved by fast burial and isolation, which ultimately requires high discharge rates and low mixing with ambient air. Recently, Trolese et al. (2019) demonstrate based on 3D numerical simulations that large volumes of welded ignimbrites often display low-height eruption columns. In these cases, the plume-air mixing is inefficient, resulting in high-temperature PDCs emplaced just a few degrees below eruption temperatures.

Welding seems to be especially prevalent in deposits of peralkaline composition, which are richer in network-modifier cations (e.g., Na^{+}, K^{+}, Ca^{2+}, Mg^{2+}), since these elements can reduce the polymerization and decreasing viscosity by several orders of magnitude, granting a higher welding window (Freundt, 1998; Grunder and Russell, 2005; Giordano et al., 2008). However, the studied samples present peraluminous to moderately metaluminous character (Barreto et al., 2014). The controversial behavior of the welded ignimbrites deposited under high temperature and viscosity conditions requires additional parameters to explain the welding foliations that are indicative of high flow-mobility. As explored in the eruption dynamics section, the presence of residual magmatic water could facilitate welding in the studied samples by considerably lowering the T_G by several degrees (Table 3; Fig. 10A, 10B), as predicted by previous models and experiments (Giordano et al, 2004, 2006, 2008).

5.2.2. Effusive deposits

The data obtained in this study show that the andesitic magmas of the Igarapé Paboca Formation possibly had low mobility, due to their physical characteristics which include a high percentage of phenocrysts (30-50% vol) and high content of microlites (Fig. 8), which is supported by viscosity estimations (Fig. 10). The observed high viscosities in the andesitic lava flows are comparable to values observed in lava domes (Yokoyama, 2009), suggesting that the effusive episodes generated either length-limited andesitic lava flows or andesitic lava domes. As discussed above, taking into account that even a few tenths wt.% H_2O can strongly influence magma rheology (Giordano et al., 2006, 2008), a more hydrous magma condition may counterbalance the effect phenocrysts in the effusive deposits, allowing the magmatic ascent and eruption as lava flows. Unfortunately, the erosion level in the study area does not allow the verification of diagnostic field features (Silva et al., 2019), such as dome morphology or the presence of margined autoclastic breccias.

In addition to the andesites, the effusive eruptive style also generated spessartitic lamprophyres and dacites that exhibit a hypabyssal nature. This hypabyssal emplacement is explained, in the lamprophyre case, because they normally occur as dykes (Le Maitre, 2002) and, in the dacite case, because they show vertical to sub-vertical flow-foliations that can be interpreted as roots of fissural feeding systems (Fig. 4G).

5.3. Reconstruction of the volcanic environment

Despite the challenges related to this ancient volcanic setting, the field, petrographic and rheological data presented in this study allow us to provide a reconstruction of the volcanic environment that generated the extensive volcanic units present in this region. The results showed that there is a large volume of pyroclastic rocks with moderate- to high welding degrees in the studied area when compared with the effusive deposits.

It is important to note that due to the intense uplift and magmatism, only the deeper features of SLIPs may be preserved, such as caldera collapse structures, granite intrusions, and dike swarms (Bryan et al., 2002). In contrast, the tectonic stability of the Amazonian Craton from Orosirian onward, combined with arid climate conditions (Cunha, 2006) and the fast burial of the volcaniclastic units (Juliani and Fernandes, 2010) seem to have contributed to the exceptional preservation of the volcaniclastic sequences (Barreto et al., 2013; Roverato et al., 2019). Therefore, this proportion could be apparent and just refer to enabling strongly welded rocks to be better preserved instead of effusive and unwelded matrix-supported pyroclastic rocks that are easily weathered, eroded, and transported in a subaerial environment.

The textural analysis of the studied volcanic rocks indicates that the emplacement temperatures of the two Orosirian volcanic episodes of the Erepecuru-Trombetas region are progressively higher from southwest towards northeast. The first episode is recorded by the Igarapé Paboca Formation, which represents the 1.99 Ga older volcanism in the region (Barreto et al. 2013; Castro et al., 2014; Silva et al., 2019), responsible for the emplacement of subaerial explosive rocks (incipiently welded lapilli-tuffs to moderately welded ignimbrites), in association to andesitic magmatic pulses of effusive nature.

The second and main volcanic episode of 1.88 Ga (Barreto et al., 2013; Castro et al., 2014; Silva et al., 2019) reveals the existence of an expressive explosive event that produced the Iricoumé Group, marked by the presence of ignimbrites. During this episode predominated pyroclastic density currents which generated incipiently welded crystal-rich ignimbrites and rhyolitic-dacitic ignimbrites with distinct welding degrees. A late volcanic episode related to the Iricoumé Group is represented by effusive spessartitic lamprophyres and dacites that occur as dykes and crosscut the volcanic stratigraphy, which is reinforced by ages ranging from 1.99 Ga to 1.88 Ga of a dacite sample (Vianna et al., 2017).

Geochronological, geochemical, and isotopic data show that the Iricoumé Group magmatism in the Erepecuru-Trombetas took place in a post-collisional setting (Barreto et al., 2014), and is likely associated with the development of mantle plume (Teixeira et al., 2019). This setting suggests a strong structural control on the emplacement of Iricoumé Group, in which pre-existing structures would act in two ways: 1) facilitating the connection with the multiple regional magma reservoirs (Forte and Castro, 2019); 2) governing the development of calderas and fissure ignimbrite. Similar geodynamic settings have been observed in other regions of the world (e.g., Aguirre-Dıaz and Labarthe-Hernandez, 2003; Spinks et al., 2005; Robertson et al., 2015).

Under anhydrous conditions, the studied samples of the Iricoumé Group present high T_L ranging from 920 to 1110 ºC, frequently > 1000 ºC (Table 3). These values are comparable to T_L estimations for 'dry' SLIPs (Bryan et al., 2002; Simões et al., 2014b), and considerably higher when compared to other minor silicic systems in southern Brazil (Sommer et al., 2013; Santos et al., 2019; Haag et al., 2021), and around the world (e.g., Grunder, 1977; Clemens et al., 1986; King et al., 1997; Patino-Dulce, 1997; Dall'Agnol et al., 1999; Hergt et al., 2007). In contrast, the older Igarapé Paboca magmatism seems to present even higher temperatures (T_L > 1100 ºC) and a predominance of less evolved terms, such as andesites and dacites (Barreto et al., 2013; Silva et al., 2019).

In addition to that, the estimated T_{Zr} in this study agree with previous estimations performed in Iricoumé Group rocks in the Uatumã-Anauá Domain (Fig. 1B) in the Pitinga region, where T_{Zr} estimations ranged from 799 to 984 ºC (Ferron et al., 2010; Pierosan et al., 2011b; Simões et al., 2014a). These high temperatures are supported by field and petrographic data, in particular, high-temperature devitrification features and evidence of ductile deformation as a result of welding processes. The high temperature calculations obtained in this study for both effusive and explosive deposits associated with high-temperature textural features allow us to suggest a volcanic environment with high-discharge, continuous, and low eruptive column dynamics, typical of calderas and/or fissure-fed ignimbrites (Cas and Wright, 1987; Lowell, 1991; Aguirre-Dıaz and Labarthe-Hernandez, 2003).

Polyphase evolution with alternation of both effusive and explosive pulses is a common feature in caldera-related environments (Lipman, 1984, 2000) and has been described in other domains of the Amazonian Craton (Pierosan, et al. 2011; Lagler et al., 2019) and the Paleoproterozoic Kaapvaal craton (Oberholzer and Eriksson, 2000). Due to the extensive occurrence of explosive rocks related to the Iricoumé Group (mainly welded ignimbrites) and analog units in the Amazonian Craton, a few calderas have been proposed as possible sources for these rocks (e.g., Ferron et al., 2010; Pierosan et al., 2011b; Lagler et al., 2019). Most of these putative calderas have been proposed based on geomorphologic attributes, such as relief and drainage patterns since access to most of these areas is still difficult (Pierosan et al., 2011b). However, the number of proposed calderas is still scarce when compared to the extension of more than 1.2 million km^2 of outcropping volcanic rocks associated with the Uatumã event (Roverato et al., 2016).

The apparent absence of caldera-collapse structures in the Erepecuru-Trombetas region, along with structural and field evidence, led us to an alternative hypothesis involving fissure-fed ignimbrites for the emplacement of the studied rocks in the region (*sensu* Aguirre-Dıaz and Labarthe-Hernandez, 2003). This environment for the generation of the volcanic sequences has been proposed for the Tapajós and Iriri-Xingu domains, both located in the southern Amazonian Craton (e.g., Juliani and Fernandes, 2010; Roverato et al., 2019). In this model, regional faults act as conduits, yielding high-temperature and voluminous ignimbrite sequences followed by aligned rhyolitic lava domes (Aguirre-Dıaz and Labarthe-Hernandez, 2003; Juliani and Fernandes, 2010).

Estimations of pressure and oxygen fugacity for calcic amphiboles performed by Pierosan et al. (2011a) in the Pitinga region (Uatumã-Anauá Domain; Fig. 1) indicate pressure conditions of 0.5 to 1.0 kbar and depths of ~ 2 Km, compatible with shallow magma chambers (Walker, 2008). At the time of the Uatumã magmatism emplacement, lithospheric thinning and extension related to mantle plume impact in the lithosphere would result in axial faults and the development of basin and range structures, exploiting pre-existing collisional structures. These faults can reach depths of 20 km (Hamilton, 1987) that could easily connect with the shallow magma chambers in the region, leading to sudden decompression and triggering voluminous fissural and caldera ignimbrite eruptions (Fig. 12). The presence of a strong structural control marked by NW-SE regional faults in the Erepecuru-Trombetas domain (see Fig. 2; Silva et al., 2019) could reinforce this hypothesis.

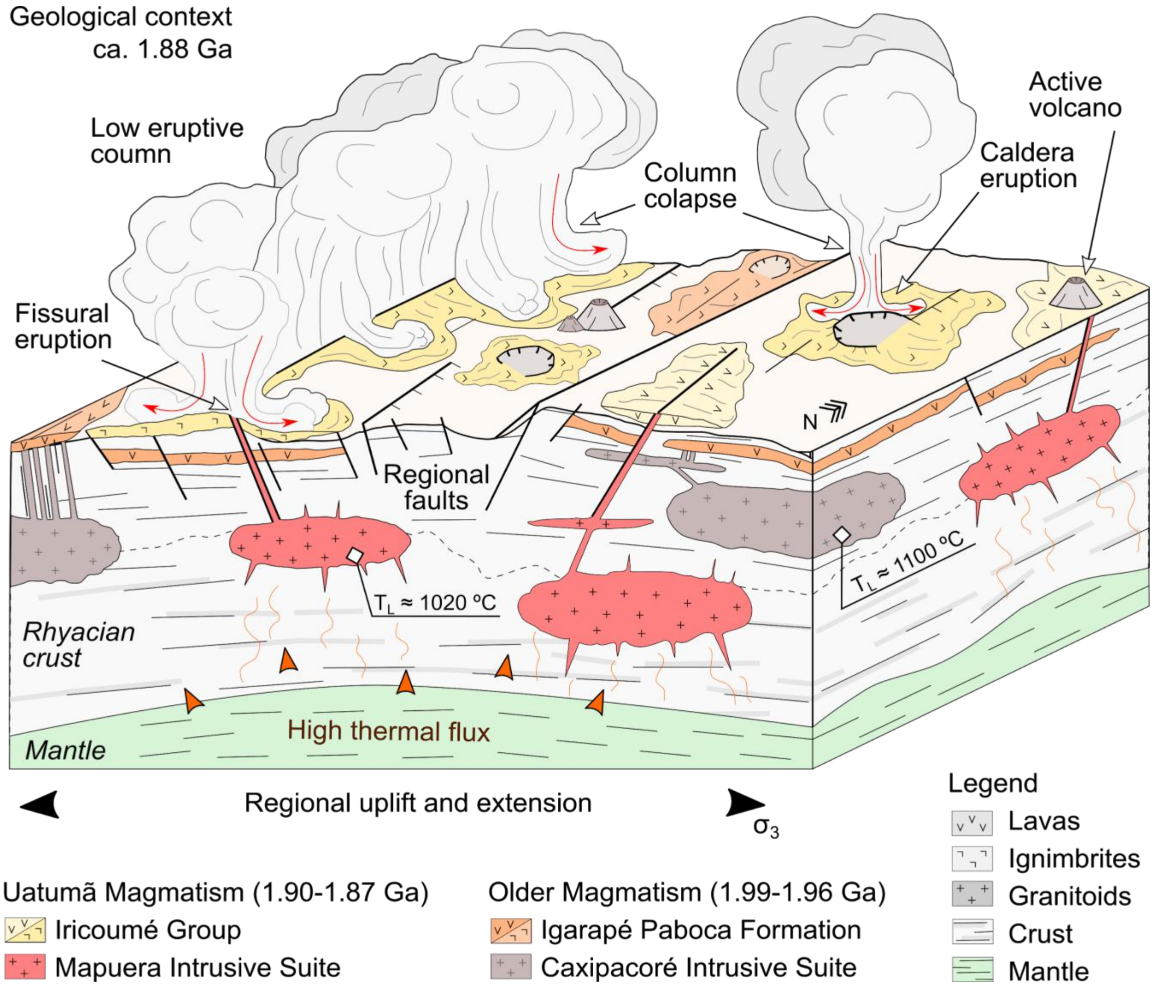

Fig. 12. Reconstruction of the volcanic history in the Erepecuru-Trombetas region: regional context in which regional faults exploit shallow magma chambers, triggering voluminous explosive fissure-fed and caldera eruptions.

6. Concluding remarks

This study indicates a large volume of pyroclastic rocks with moderate to high welding degrees in the studied area. The main results are:

1. Two Orosirian volcanic episodes predominate in the Erepecuru-Trombetas region: the 1.99 Ga Igarapé Paboca Formation (subaerial explosive rocks and effusive pulses of andesitic composition), and the 1.88 Ga Iricoumé Group (mainly composed of subaerial explosive rock). A late volcanic episode related to the Iricoumé Group is represented by effusive spessartitic lamprophyres and dacites that crosscut the volcanic stratigraphy.

2. Rheological data suggest a predominance of high temperatures for the samples of the Iricoumé Group (T_{Zr} ranging from 729 to 867 ºC) and Igarapé Paboca Formation (T_{Zr} ranging from 851 to 871 ºC). These data are supported by the textural evidences that include thermally oxidized pyroclasts, extensive welding and rheomorphism.

3. Ignimbrites show a increase in welding intensity as a function of ΔT_{Zr}-T_G. This implies a hot, gas-supported PDC emplacement and a direct association between eruption and emplacement temperatures. This suggests a volcanic environment with a high-discharge and low eruptive column dynamics and/or a proximal source, compatible with both caldera and fissure-fed ignimbrites.

4. Rheological data suggest that even small additions of H_2O can lead to a considerable decreasing of both melt viscosity and temperature (T_L and T_G), resulting in porosity loss and welding. This should accelerate the magma ascent and enhance fragmentation by decompression, as supported by petrographic evidence.

This study provides rheological boundaries and an environmental reconstruction supported by textural analysis and rheological parameter calculations. However, more detailed studies of volcanic stratigraphy with lithofacies associations are necessary to define proximal to distal facies and fully reconstruct the Orosirian volcanism in the northern Amazon Craton.

Acknowledgements

We acknowledge the CNPq/Universal project (Grant 484571/2007-9) for financial support and CPRM/Belém for taking the samples used in this study. The authors are grateful to reviews of Joan Martí, Matteo Roverato and the editor Wilson Teixeira by provided important suggestions to improvement of the manuscript.

References

Aguirre-Díaz, G.J., Labarthe-Hernández, G., 2003. Fissure ignimbrites: Fissure-source origin for voluminous ignimbrites of the Sierra Madre Occidental and its relationship with Basin and Range faulting. Geology 31, 773. https://doi.org/10.1130/g19665.1

Almeida, F.F.M., Hasui, Y., de Brito Neves, B.B., Fuck, R.A., 1981. Brazilian structural provinces: An introduction. Earth-Science Reviews 17,1–29. https://doi.org/10.1016/0012-8252(81)90003-9

Antonio, P.Y.J., 2016. Paleomagnetismo e petrogênese de unidades Paleoproterozóicas do evento Uatumã no norte do Cráton Amazônico. Ph.D. Thesis, University of São Paulo. Instituto de Astronomia, Geofísica e Ciências Atmosféricas, 289 p.

Antonio, P.Y.J., D'Agrella-Filho, M.S., Trindade, R.I.F., Nédélec, A., de Oliveira, D.C., da Silva, F.F., Roverato, M., Lana, C., 2017. Turmoil before the boring billion: Paleomagnetism of the 1880–1860 Ma Uatumã event in the Amazonian craton. Gondwana Research 49, 106–129. https://doi.org/10.1016/j.gr.2017.05.006

Barreto, C.J.S., Lafon, J.M., Rosa Costa, L.T., Lima, E.F. de, 2013. Vulcanismo félsico paleoproterozoico do Grupo Iricoumé, Domínio Erepecuru-Trombetas, Província Amazônia Central: dados de campo, caracterização petrográfica e geocronologia Pb-Pb em zircão. Geologia USP. Série Científica 13, 47–72. https://doi.org/10.5327/z1519-874x2013000100004

Barreto, C.J.S., Lafon, J.M., Rosa Costa, L.T., Lima, E.F., 2014. Palaeoproterozoic (~1.89 Ga) felsic volcanism of the Iricoumé Group, Guyana Shield, South America: geochemical and Sm-Nd isotopic constraints on sources and tectonic environment. International Geology Review 56, 1332–1356. https://doi.org/10.1080/00206814.2014.930800

Bettencourt, J.S., Juliani, C., Xavier, R.P., Monteiro, L.V.S., Bastos Neto, A.C., Klein, E.L., Assis, R.R., Leite, W.B., Jr., Moreto, C.P.N., Fernandes, C.M.D., Pereira, V.P., 2016. Metallogenetic systems associated with granitoid magmatism in the Amazonian Craton: An overview of the present level of understanding and exploration significance. Journal of South American Earth Sciences 68, 22–49. https://doi.org/10.1016/j.jsames.2015.11.014

Branney, M.J., Kokelaar, P. 2002. Pyroclastic Density Currents and the Sedimentation of Ignimbrites. Geological Society, London, Memoirs 27.

Breitkreuz, C., 2013. Spherulites and lithophysae - 200 years of investigation on high-temperature crystallization domains in silica-rich volcanic rocks. Bull Volcanol 75. https://doi.org/10.1007/s00445-013-0705-6

Brito Neves, B.B., 2011. The Paleoproterozoic in the South- American continent: Diversity in the geologic time: Journal of South American Earth Sciences 32, 270–286. https://doi.org/10.1016/j.jsames.2011.02.004

Bryan, S.E., Ferrari, L., 2013. Large igneous provinces and silicic large igneous provinces: Progress in our understanding over the last 25 years. Geological Society of America Bulletin 125, 1053–1078. https://doi.org/10.1130/b30820.1

Bryan, S.E., Riley, T.R., Jerram, D.A., Stephens, C.J., Leat, P.T., 2002. Silicic volcanism: An undervalued component of large igneous provinces and volcanic rifted margins, in: Volcanic Rifted Margins. Geological Society of America. https://doi.org/10.1130/0-8137-2362-0.97

Cáceres, F., Wadsworth, F.B., Scheu, B., Colombier, M., Madonna, C., Cimarelli, C., Hess, K.-U., Kaliwoda, M., Ruthensteiner, B., Dingwell, D.B., 2020. Can nanolites enhance eruption explosivity? Geology. https://doi.org/10.1130/g47317.1

Cordani, U.G., Ramos, V.A., Fraga, L.M., Cegarra, M., Delgado, I., Souza, K.G., Gomes, F.E.M., Schobbenhaus, C., 2016. Tectonic map of South America, Commission For The Geological Map of the World, Map, scale 1:5.000.000.

Costa, A., 2005. Viscosity of high crystal content melts: Dependence on solid fraction. Geophysical Research Letters 32. https://doi.org/10.1029/2005gl024303

Costa, A., Caricchi, L., Bagdassarov, N., 2009. A model for the rheology of particle-bearing suspensions and partially molten rocks. Geochemistry, Geophysics, Geosystems 10. https://doi.org/10.1029/2008gc002138

Di Genova, D., Kolzenburg, S., Wiesmaier, S., Dallanave, E., Neuville, D.R., Hess, K.U., Dingwell, D.B., 2017. A compositional tipping point governing the mobilization and eruption style of rhyolitic magma. Nature 552, 235–238. https://doi.org/10.1038/nature24488

Ernst, R.E., Buchan, K.L., 2001. Large mafic magmatic events through time and links to mantle-plume heads, in: Mantle Plumes: Their Identification through Time. Geological Society of America. https://doi.org/10.1130/0-8137-2352-3.483

Fernandes, C.M.D., Juliani, C., Monteiro, L.V.S., Lagler, B., Echeverri Misas, C.M., 2011. High-K calc-alkaline to A-type fissure-controlled volcano-plutonism of the São Félix do Xingu region, Amazonian craton, Brazil: Exclusively crustal sources or only mixed Nd model ages? Journal of South American Earth Sciences 32, 351–368. https://doi.org/10.1016/j.jsames.2011.03.004

Fernandes, C.M.D., Lamarão, C.N., Teixeira, N.P., 2006. O vulcanismo bimodal do tipo Uatumã da região de São Félix do Xingu (PA). Província Mineral de Carajás. Revista Brasileira de Geociências 36, 565–576 (in Portuguese).

Ferron, J.M.T.M., Bastos Neto, A.C., Lima, E.F., Costi, H.T., Moura, C.A.V., Prado, M., Pierosan, R., Galarza, M.A., 2006. Geologia e geocronologia Pb–Pb de rochas graníticas e vulcânicas ácidas a intermediárias Paleoproterozóicas da Província Pitinga, Craton Amazônico. Revista Brasileira de Geociências 36, 501–519 (in Portuguese).

Ferron, J.M.T.M., Bastos Neto, A.C., Lima, E.F., Nardi, L.V.S., Costi, H.T., Pierosan, R., Prado, M., 2010. Petrology, geochemistry, and geochronology of Paleoproterozoic volcanic and granitic rocks (1.89–1.88Ga) of the Pitinga Province, Amazonian Craton, Brazil. Journal of South American Earth Sciences 29, 483–497. https://doi.org/10.1016/j.jsames.2009.05.001

Forte, P., Castro, J.M., 2019. H2O-content and temperature limit the explosive potential of rhyolite magma during Plinian eruptions. Earth and Planetary Science Letters 506, 157–167. https://doi.org/10.1016/j.epsl.2018.10.041

Fraga, L.M.B., Cordani, U.G., 2019. Early Orosirian tectonic evolution of the Central Guiana Shield: insights from new U-Pb SHRIMP data. In: 11th Inter Guiana Geological Conference: Tectonics and Metallogenesis of NE South America. Paramaribo, Suriname, Geologisch Mijnbouwkundige Dienst Suriname. Mededeling 29, 59-62.

Giordano, D., Nichols, A.R.L., Dingwell, D.B., 2005. Glass transition temperatures of natural hydrous melts: a relationship with shear viscosity and implications for the welding process. Journal of Volcanology and Geothermal Research 142, 105–118. https://doi.org/10.1016/j.jvolgeores.2004.10.015

Giordano, D., Russell, J.K., Dingwell, D.B., 2008. Viscosity of magmatic liquids: A model. Earth and Planetary Science Letters 271(1–4), 123–134. https://doi.org/10.1016/j.epsl.2008.03.038

Gonnermann, H.M., Manga, M., Fagents, S.A., 2013. Dynamics of magma ascent in the volcanic conduit, in: Gregg, T.K.P., Lopes, R.M.C. (Eds.), Modeling Volcanic Processes. Cambridge University Press, pp. 55–84. https://doi.org/10.1017/cbo9781139021562.004

Haag, M.B., de Freitas, R.B., Sommer, C.A., Savian, J.F., Lima, E.F., Gambeta, J.H., Lyra, D. da S., Trindade, R.I.F. da, 2021. Multi-proxy case study of a Neoproterozoic rhyolite flow in southernmost Brazil: Emplacement mechanisms and implications for ancient felsic lavas. Journal of South American Earth Sciences 107, 102982. https://doi.org/10.1016/j.jsames.2020.102982

Hamilton, W., 1987. Crustal extension in the Basin and Range Province, southwestern United States. Geological Society, London, Special Publications 28, 155–176. https://doi.org/10.1144/gsl.sp.1987.028.01.12

Juliani, C., Fernandes, C.M.D., 2010. Well-preserved Late Paleoproterozoic volcanic centers in the São Félix do Xingu region, Amazonian Craton, Brazil. Journal of Volcanology and Geothermal Research 191, 167–179. https://doi.org/10.1016/j.jvolgeores.2010.01.016

Juliani, C., Fernandes, C.M.D., Monteiro, L.V.S., Lagler, B., Misas, C.M.E., 2011. Very low-grade metamorphism and very well preserved epithermal mineralization in the Paleproterozoic Uatumã LIP, Southern Amazonian craton, Brazil: European Geosciences Union General Assembly, Abstracts, p. 11815.

Klein, E.L., Almeida, M.E., Costa, L.T.R., 2012. The 1.89- 1.87 Ga Uatumã Silicic Large Igneous Province, northern South America: Large Igneous Provinces Commission: http://www.largeigneousprovinces.org/12nov (accessed 10 July 2020).

Kohn, S.C., 2000. The dissolution mechanisms of water in silicate melts; a synthesis of recent data. Mineralogical Magazine 64, 389–408. https://doi.org/10.1180/002646100549463

Lagler, B., Juliani, C., Dias Fernandes, C.M., Souza da Cruz, R., Strauss Vieira, D.A., 2019. Paleoproterozoic volcanic caldera in the Amazonian craton, northern Brazil: Stratigraphy, lithofacies characterization, and lithogeochemical constraints. Journal of South American Earth Sciences 95, 102252. https://doi.org/10.1016/j.jsames.2019.102252

Lamarão, C.N., Dall'Agnol, R., Lafon, J.-M., Lima, E.F., 2002. Geology, geochemistry, and Pb–Pb zircon geochronology of the Paleoproterozoic magmatism of Vila Riozinho, Tapajós Gold Province, Amazonian craton, Brazil. Precambrian Research 119, 189–223. https://doi.org/10.1016/s0301-9268(02)00123-7

Liu, H.-Q., Xu, Y.-G., He, B., 2013. Implications from zircon-saturation temperatures and lithological assemblages for Early Permian thermal anomaly in northwest China. Lithos 182–183, 125–133. https://doi.org/10.1016/j.lithos.2013.09.015

Magalhães, L.B., Lafon, J.M., Rosa-Costa, L.T., Barreto, C.J.S., Dantas, E.L., 2017. Geocronologia de zircões detríticos por LA-ICP-MS de cobertura sedimentar

Paleoproterozoica do Dominio Erepecuru-Trombetas Oeste, Província Amazônia Central. In: Anais do 15º Simpósio de Geologia da Amazônia, Belém. p. 447-450.

Manville, V., Németh, K., Kano, K., 2009. Source to sink: A review of three decades of progress in the understanding of volcaniclastic processes, deposits, and hazards. Sedimentary Geology 220, 136–161. https://doi.org/10.1016/j.sedgeo.2009.04.022

Motta, J.G., Souza Filho, C.R. de, Carranza, E.J.M., Braitenberg, C., 2019. Archean crust and metallogenic zones in the Amazonian Craton sensed by satellite gravity data. Scientific Reports 9. https://doi.org/10.1038/s41598-019-39171-9

Muller, A., Breiter, K., Seltmann, R., Pécskay, Z. 2005. Quartz and feldspar zoning in the eastern Erzgebirge volcano-plutonic complex (Germany, Czech Republic): evidence of multiple magma mixing. Lithos 80, 201-227. https://doi.org/10.1016/j.lithos.2004.05.011

Muller, A., René, M., Behr, H.J., Kronz, A. 2003. Trace elements and cathodoluminescence of igneous quartz in topaz granites from the Hub Stock (Slavkovský Les Mts., Czech Republic). Mineralogy and Petrology 79, 167-191. https://doi.org/10.1007/s00710-003-0238-3

Pacheco-Hoyos, J.G., Aguirre-Díaz, G.J., Dávila-Harris, P., 2017. Boiling-over dense pyroclastic density currents during the formation of the ~ 100 km3 Huichapan ignimbrite in Central Mexico: Stratigraphic and lithofacies analysis. Journal of Volcanology and Geothermal Research 349, 268–282. https://doi.org/10.1016/j.jvolgeores.2017.11.007

Pierosan, R., de Lima, E.F., Nardi, L.V.S., Bastos Neto, A.C., de Campos, C.P., Jarvis, K., Ferron, J.M.T.M., Prado, M., 2011a. Geochemistry of Palaeoproterozoic volcanic rocks of the Iricoumé Group, Pitinga Mining District, Amazonian craton, Brazil. International Geology Review 53, 946–979. https://doi.org/10.1080/00206810903391542

Pierosan, R., Lima, E.F., Nardi, L.V.S., Campos, C.P., Bastos Neto, A.C., Ferron, J.M.T.M., Prado, M., 2011b. Paleoproterozoic (~1.88Ga) felsic volcanism of the Iricoumé Group in the Pitinga Mining District area, Amazonian Craton, Brazil: insights in ancient volcanic processes from field and petrologic data. Anais da Academia Brasileira de Ciências 83 (3), 921–937. http://dx.doi.org/10.1590/S0001-37652011000300012

Pinho, S.C.C., Fernandes, C.M.D., Teixeira, N.P., Paiva Jr., A.L., Cruz, V.L., Lamarão, C.N., Moura, C.A.V., 2006. O magmatismo paleoproterozóico da região de São Félix do Xingu, Província Estanífera do Sul do Pará: Petrografia e Geocronologia. Revista Brasileira de Geociências 36, 793–802 (in Portuguese).

Quane, S.L., Russell, J.K., 2004. Ranking welding intensity in pyroclastic deposits. Bulletin of Volcanology 67, 129–143. https://doi.org/10.1007/s00445-004-0367-5

Reis, N.J., Almeida, M.E., Riker, S.R.L., Ferreira, A.L., 2006. Geologia e Recursos minerais do Estado do Amazonas, Manaus: CPRM, (Convênio CPRM/CIAMA). 125 p., il. Escala 1:1.000.000.

Reis, N.J., Fraga, L.M., Faria, M.S.G., and Almeida, M.E., 2003. Geologia do Estado de Roraima, Brasil: Geology of France and Surrounding Areas- Special Guiana Shield, v. 2-3-4, p. 121–134.

Robertson, E.A.M., Biggs, J., Cashman, K.V., Floyd, M.A., Vye-Brown, C., 2015. Influence of regional tectonics and pre-existing structures on the formation of elliptical calderas in the Kenyan Rift. Geological Society, London, Special Publications 420, 43–67. https://doi.org/10.1144/sp420.12

Roverato, M., 2016. The Montesbelos mass-flow (southern Amazonian craton, Brazil): a Paleoproterozoic volcanic debris avalanche deposit? Bull Volcanol 78. https://doi.org/10.1007/s00445-016-1043-2

Roverato, M., Giordano, D., Echeverri-Misas, C.M., Juliani, C., 2016. Paleoproterozoic felsic volcanism of the Tapajós Mineral Province, Southern Amazon Craton, Brazil. Journal of Volcanology and Geothermal Research 310, 98–106. https://doi.org/10.1016/j.jvolgeores.2015.11.019

Roverato, M., Juliani, C., Dias-Fernandes, C.M., Capra, L., 2017. Paleoproterozoic andesitic volcanism in the southern Amazonian craton, the Sobreiro Formation: New insights from lithofacies analysis of the volcaniclastic sequences. Precambrian Research 289, 18–30. https://doi.org/10.1016/j.precamres.2016.11.005

Roverato, M., Giordano, D., Giovanardi, T., Juliani, C., Polo, L., 2019. The 2.0–1.88 Ga Paleoproterozoic evolution of the southern Amazonian Craton (Brazil): An interpretation inferred by lithofaciological, geochemical and geochronological data. Gondwana Research 70, 1–24. https://doi.org/10.1016/j.gr.2018.12.005

Santos, J.O.S., Groves, D.I., Hartmann, L.A., Moura, M.A., McNaughton, N.J., 2001. Gold deposits of the Tapajós and Alta Floresta Domains, Tapajós–Parima orogenic belt, Amazon Craton, Brazil. Mineralium Deposita 36, 278–299. https://doi.org/10.1007/s001260100172

Santos, J.O.S., Hartmann, L.A., Faria, M.S., Riker, S.R., Souza, M.M., Almeida, M.E., McNaugthon, N.J., 2006. A compartimentação do cráton amazonas em províncias: avanços ocorridos no período 2000–2006, in Simpósio de Geologia da Amazônia, 9th, Atas.

Santos, J.O.S., Hartmann, L.A., Gaudette, H.E., Groves, D.I., Mcnaughton, N.J., Fletcher, I.R., 2000. A New Understanding of the Provinces of the Amazon Craton Based on Integration of Field Mapping and U-Pb and Sm-Nd Geochronology. Gondwana Research 3, 453–488. https://doi.org/10.1016/s1342-937x(05)70755-3

Santos, E.A. dos, Sommer, C.A., Waichel, B.L., Haag, M.B., 2019. Ediacaran post-collisional high-silica volcanism associated to the Florianópolis Batholith, Dom Feliciano Belt, southernmost Brazil: lithofacies analysis and petrology. Journal of South American Earth Sciences 96, 102299. https://doi.org/10.1016/j.jsames.2019.102299

Schindelin, J., Arganda-Carreras, I., Frise, E., Kaynig, V., Longair, M., Pietzsch, T., Preibisch, S., Rueden, C., Saalfeld, S., Schmid, B., Tinevez, J.-Y., White, D.J., Hartenstein, V., Eliceiri, K., Tomancak, P., Cardona, A., 2012. Fiji: an open-source platform for biological-image analysis. Nature Methods 9, 676–682. https://doi.org/10.1038/nmeth.2019

Schobbenhaus, C., Brito Neves, B.B., 2003. A Geologia do Brasil no Contexto da Plataforma Sul-Americana, in Bizzi, L.A., Schobbenhaus, C., Vidotti, R.M., and Gonçalves, J.H., eds., Geologia, tectônica e Recursos Minerais do Brasil: Brasília, CPRM, p. 5–53.

Silva, R.C.S., Castro, J.M.R., Rosa-Costa, L.T., Chaves, C.L., 2019. Geologia e recursos minerais da folha Rio Trombetas SA.21-X-A, estado do Pará: texto-explicativo, CPRM, Map, Scale 1:250.000. Available at: http://rigeo.cprm.gov.br/jspui/handle/doc/21492

Simões, M.S., Almeida, M.E., de Souza, A.G.H., da Silva, D.P.B., Rocha, P.G., 2014a. Characterization of the volcanic and hypabissal rocks of the Paleoproterozoic Iricoumé

Group in the Pitinga region and Balbina Lake area, Amazonian Craton, Brazil: Petrographic distinguishing features and emplacement conditions. Journal of Volcanology and Geothermal Research 286, 138–147. https://doi.org/10.1016/j.jvolgeores.2014.08.024

Simões, M.S., Rossetti, L. de M.M., Lima, E.F. de, Ribeiro, B.P., 2014b. The role of viscosity in the emplacement of high-temperature acidic flows of Serra Geral Formation in Torres Syncline (Rio Grande do Sul State, Brazil). Brazilian Journal of Geology 44, 669–679. https://doi.org/10.5327/z23174889201400040010

Sisson, T.W., Grove, T.L., 1993. Temperatures and H2O contents of low-MgO high-alumina basalts. Contributions to Mineralogy and Petrology 113(2), 167–184. https://doi.org/10.1007/bf00283226

Soriano, C., Zafrilla, S., Martí, J., Bryan, S., Cas, R., Ablay, G., 2002. Welding and rheomorphism of phonolitic fallout deposits from the Las Cañadas caldera, Tenerife, Canary Islands. Geological Society of America Bulletin 114, 883–895. https://doi.org/10.1130/0016-7606(2002)114<0883:waropf>2.0.co;2

Spinks, K.D., Acocella, V., Cole, J.W., Bassett, K.N., 2005. Structural control of volcanism and caldera development in the transtensional Taupo Volcanic Zone, New Zealand. Journal of Volcanology and Geothermal Research 144, 7–22. https://doi.org/10.1016/j.jvolgeores.2004.11.014

Tassinari, C.C.G., Macambira, M.J.B., 2004, A evolução tectônica do Cráton Amazônico, in Mantesso Neto, V., Bartorelli, A., Dal Ré Carneiro, C., and de Brito Neves, B.B., eds., Geologia do continente Sul-Americano: evolução da obra de Fernando Flávio Marques de Almeida: São Paulo, Beca, p. 471–485.

Teixeira, W., Nelson, J.R., Bettencourt, J.S., Klein, E.L., Oliveira, D.C., 2019. Intraplate Proterozoic magmatism in the Amazonian Craton reviewed: geochronology, crustal tectonics and global matches. Dyke Swarms of the World: A Modern Perspective https://doi.org/10.1007/978-981-13-1666-1_4

Vasquez, M.L., Costa, L.T.R., 2008, Mapa Geológico e de Recursos Minerais do Estado do Pará. Projeto Geologia e Recursos Minerais do Pará – Sistema de Informações Geográficas: texto-explicativo, Belém, CPRM, Mapa, col. Escala 1:1.000.000. 1 CD-ROM.

Vernon, R.H. 2004. A practical guide to Rock Microstructure. Cambridge University Press, New York, p. 655.

Vianna, S.Q., Magalhães, L.B., Lafon, J.M., Rosa-Costa, L.T. 2017. Geocronologia U-Pb e Pb-Pb e geoquímica isotópica Sr-Nd da porção oeste do Domínio Erepecuru - Trombetas, Província Amazônia Central, noroeste do Pará. In: Anais do 15º Simpósio de Geologia da Amazônia, Belém. p. 451-454.

Walter, T.R., 2008. Chapter 9 Facilitating Dike Intrusions into Ring-Faults, in: Caldera Volcanism: Analysis, Modelling and Response. Elsevier, pp. 351–374. https://doi.org/10.1016/s1871-644x(07)00009-5

Watson, E.B., 1979. Zircon saturation in felsic liquids: Experimental results and applications to trace element geochemistry. Contributions to Mineralogy and Petrology 70, 407–419. https://doi.org/10.1007/bf00371047

Watson, E.B., Harrison, T.M., 1983. Zircon saturation revisited: temperature and composition effects in a variety of crustal magma types. Earth and Planetary Science Letters 64, 295–304. https://doi.org/10.1016/0012-821x(83)90211-x

Webb, S., 1997. Silicate melts: Relaxation, rheology, and the glass transition. Reviews of Geophysics 35, 191–218. https://doi.org/10.1029/96rg03263

Yokoyama, I., 2009. Growth rates of lava domes with respect to viscosity of magmas. Annals of Geophysics 48. https://doi.org/10.4401/ag-3246